Protein phosphatase 2A holoenzymes regulate leucine-rich repeat kinase 2 phosphorylation and accumulation

Matthieu Drouyer, Marc F. Bolliger, Evy Lobbestael, Chris van den Haute, Marco Emanuele, Réginald Lefebvre, William Sibran, Tina de Wit, Coline Leghay, Eugénie Mutez, et al.

▶ **To cite this version:**

Matthieu Drouyer, Marc F. Bolliger, Evy Lobbestael, Chris van den Haute, Marco Emanuele, et al.. Protein phosphatase 2A holoenzymes regulate leucine-rich repeat kinase 2 phosphorylation and accumulation. Neurobiology of Disease, 2021, 157, pp.105426. 10.1016/j.nbd.2021.105426 . hal-03373115

HAL Id: hal-03373115
https://hal.univ-lille.fr/hal-03373115v1

Submitted on 12 Oct 2021

HAL is a multi-disciplinary open access archive for the deposit and dissemination of scientific research documents, whether they are published or not. The documents may come from teaching and research institutions in France or abroad, or from public or private research centers.

L'archive ouverte pluridisciplinaire **HAL**, est destinée au dépôt et à la diffusion de documents scientifiques de niveau recherche, publiés ou non, émanant des établissements d'enseignement et de recherche français ou étrangers, des laboratoires publics ou privés.

Distributed under a Creative Commons Attribution - NonCommercial - NoDerivatives 4.0 International License

Neurobiology of Disease 157 (2021) 105426

Contents lists available at ScienceDirect

Neurobiology of Disease

journal homepage: www.elsevier.com/locate/ynbdi

Protein phosphatase 2A holoenzymes regulate leucine-rich repeat kinase 2 phosphorylation and accumulation

Matthieu Drouyer [a,b,1,2], Marc F. Bolliger [c,1,3], Evy Lobbestael [d,1], Chris Van den Haute [d,e], Marco Emanuele [a,b], Réginald Lefebvre [a,b], William Sibran [a,b], Tina De Wit [d], Coline Leghay [a,b], Eugénie Mutez [a,b], Nicolas Dzamko [f,g], Glenda M. Halliday [f,g], Shigeo Murayama [h], Alain Martoriati [i], Katia Cailliau [i], Jean-François Bodart [i], Marie-Christine Chartier-Harlin [a,b,*,4], Veerle Baekelandt [d,*,4], R. Jeremy Nichols [c,j,**,4], Jean-Marc Taymans [a,b,d,***,4]

[a] Université de Lille, Inserm, CHU Lille, UMR-S1172, LilNCog, Lille Neuroscience & Cognition, 59000 Lille, France
[b] Inserm, UMR-S 1172, Team "Brain Biology and Chemistry", 59000 Lille, France
[c] Parkinson's Institute and Clinical Center, Sunnyvale, CA 94085, USA
[d] KU Leuven, Laboratory for Neurobiology and Gene Therapy, Department of Neurosciences, 3000 Leuven, Belgium
[e] Leuven Viral Vector Core, KU Leuven, Leuven, Belgium
[f] Central Clinical School, University of Sydney, Camperdown, NSW 2050, Australia
[g] School of Medical Sciences, University of NSW, Kensington, NSW 2033, Australia
[h] Department of Neuropathology, Brain Bank for Aging Research, Tokyo Metropolitan Geriatric Hospital, Tokyo 173-0015, Japan
[i] Univ. Lille, CNRS, UMR 8576-UGSF-Unité de Glycobiologie Structurale et Fonctionnelle, F-59000 Lille, France
[j] Department of Pathology, Stanford University School of Medicine, Palo Alto, CA 94305, USA

ARTICLE INFO

Keywords:
LRRK2
Phosphatases
Phosphorylation
Ubiquitination
Parkinson's disease
PP2A
CRISPRi

ABSTRACT

LRRK2 is a highly phosphorylated multidomain protein and mutations in the gene encoding LRRK2 are a major genetic determinant of Parkinson's disease (PD). Dephosphorylation at LRRK2's S910/S935/S955/S973 phosphosite cluster is observed in several conditions including in sporadic PD brain, in several disease mutant forms of LRRK2 and after pharmacological LRRK2 kinase inhibition. However, the mechanism of LRRK2 dephosphorylation is poorly understood.

We performed a phosphatome-wide reverse genetics screen to identify phosphatases involved in the dephosphorylation of the LRRK2 phosphosite S935. Candidate phosphatases selected from the primary screen were tested in mammalian cells, *Xenopus* oocytes and in vitro. Effects of PP2A on endogenous LRRK2 phosphorylation were examined via expression modulation with CRISPR/dCas9.

Our screening revealed LRRK2 phosphorylation regulators linked to the PP1 and PP2A holoenzyme complexes as well as CDC25 phosphatases. We showed that dephosphorylation induced by different kinase inhibitor

Abbreviations: ANK, ankyrin repeat; CRISPR, clustered interspaced short palindromic repeats; CRISPRi, CRISPR interference; DLB, dementia with Lewy body; DUSP, dual specificity phosphatase; GWAS, genome-wide association studies; LRR, leucine-rich repeat; LRRK2, leucine-rich repeat kinase 2; LV, lentiviral; PD, Parkinson's disease; PLA, Proximity ligation assay; PP1, Protein phosphatase 1; PP2A, Protein phosphatase 2A; PPP, phosphoprotein phosphatase (serine/threonine); PTP, protein tyrosine phosphatase; TSS, Transcription Start Site.

* Corresponding authors.
** Correspondence to: R. Jeremy Nichols, Department of Pathology, Stanford University School of Medicine, Palo Alto, CA 94305, USA.
*** Correspondence to: Jean-Marc Taymans, Université de Lille, Inserm, CHU Lille, UMR-S1172, LilNCog, Lille Neuroscience & Cognition, 59000 Lille, France.
E-mail addresses: mdrouyer@cmri.org.au (M. Drouyer), evy.lobbestael@kuleuven.be (E. Lobbestael), chris.vandenhaute@kuleuven.be (C. Van den Haute), william.sibran@inserm.fr (W. Sibran), coline.leghay@inserm.fr (C. Leghay), eugenie.mutez@chru-lille.fr (E. Mutez), nicolas.dzamko@sydney.edu.au (N. Dzamko), glenda.halliday@sydney.edu.au (G.M. Halliday), alain.martoriati@univ-lille.fr (A. Martoriati), katia.maggio@univ-lille.fr (K. Cailliau), jean-francois.bodart@univ-lille.fr (J.-F. Bodart), marie-christine.chartier-harlin@inserm.fr (M.-C. Chartier-Harlin), veerle.baekelandt@kuleuven.be (V. Baekelandt), rjnichols@stanford.edu (R.J. Nichols), jean-marc.taymans@inserm.fr (J.-M. Taymans).
[1] Equal contributors.
[2] Current affiliation: Children's Medical Research Institute, Westmead, Australia.
[3] Current affiliation ESCAPE Bio, South San Francisco, CA 94080, USA.
[4] Shared senior authorship.

https://doi.org/10.1016/j.nbd.2021.105426
Received 3 December 2020; Received in revised form 9 June 2021; Accepted 10 June 2021
Available online 16 June 2021
0969-9961/© 2021 Published by Elsevier Inc. This is an open access article under the CC BY-NC-ND license (http://creativecommons.org/licenses/by-nc-nd/4.0/).

triggered relocalisation of phosphatases PP1 and PP2A in LRRK2 subcellular compartments in HEK-293 T cells. We also demonstrated that LRRK2 is an authentic substrate of PP2A both in vitro and in *Xenopus* oocytes. We singled out the PP2A holoenzyme PPP2CA:PPP2R2 as a powerful phosphoregulator of pS935-LRRK2. Furthermore, we demonstrated that this specific PP2A holoenzyme induces LRRK2 relocalization and triggers LRRK2 ubiquitination, suggesting its involvement in LRRK2 clearance. The identification of the PPP2CA:PPP2R2 complex regulating LRRK2 S910/S935/S955/S973 phosphorylation paves the way for studies refining PD therapeutic strategies that impact LRRK2 phosphorylation.

1. Introduction

Mutations in the *leucine-rich repeat kinase 2* (*LRRK2*) gene are one of the most prevalent causes of monogenic PD (Zimprich et al., 2004) with several mutant forms of LRRK2 segregating with disease, including N1437H, R1441C/G/H, Y1699C, G2019S and I2020T (Nichols et al., 2010). LRRK2 mutations are also present in apparently sporadic cases of PD, with a prevalence of 2% to up to 40% in certain populations. In addition, LRRK2 was genetically associated to PD in several independent genome-wide association studies (GWAS) (Simón-Sánchez et al., 2009; Satake et al., 2009; Lill et al., 2012). Moreover, PD patients carrying the LRRK2 mutations, such as the G2019S mutation in the LRRK2 kinase domain, show a clinical and neuropathological profile that is very similar to sporadic PD (Healy et al., 2008; Haugarvoll et al., 2008), indicating that LRRK2 contributes to a PD disease pathway common to both familial and sporadic PD. Finally, LRRK2 kinase activity is shown to be activated in both familial and sporadic PD (Taymans and Greggio, 2016; Di Maio et al., 2018) making LRRK2 a priority therapeutic target for novel disease-modifying therapies for PD.

LRRK2 is a complex protein of 2527 amino acids containing several predicted functional domains consisting of a ROC-type GTPase domain as well as a serine/threonine protein kinase domain (Mata et al., 2006). LRRK2 is highly phosphorylated with two notable classes of phosphorylation sites, one of autophosphorylation sites clustering in or near LRRK2's Ras-GTPase-like domain (termed ROC) and another of heterologous phosphorylation sites in the N-terminal ANK-LRR interdomain region (Gloeckner et al., 2010). Evidence of a physiological role for LRRK2 phosphorylation has accumulated in recent years for those phosphosites of the N-terminal region, especially at positions S910, S935, S955 and S973. Phosphorylation levels at these sites are reduced for several pathogenic mutants such as N1437H, R1441C/G, Y1699C and I2020T compared to wild type LRRK2 when expressed in cell culture or animal models (Nichols et al., 2010; Dzamko et al., 2010; Doggett et al., 2012; Lobbestael et al., 2013). Also, all of these sites are rapidly dephosphorylated upon LRRK2 inhibitor treatment, considered as a potential therapeutic approach.

Interestingly dephosphorylation of the phosphosites of the LRRK2 N-terminal region in the presence of LRRK2 PD mutations or inhibition of LRRK2 led to similar cellular LRRK2 phenotypes such as its accumulation in cytoplasmic inclusions and filamentous skein-like structures, loss of 14–3-3 binding and increased binding of PP1 in cell (and animal) models (Nichols et al., 2010; Lobbestael et al., 2013; Li et al., 2011). In addition, phosphorylation at these sites is reduced in PD brains (Dzamko et al., 2017), suggesting that LRRK2 dephosphorylation is linked to PD pathogenesis. Furthermore, phosphoregulation of these sites indirectly regulates LRRK2 substrate phosphorylation (Ito et al., 2016; Kalogeropulou et al., 2018), and therefore the kinases and phosphatases that modify LRRK2 are prime targets for elucidation.

To date, several studies have reported kinases phosphorylating LRRK2 including casein kinase 1α, cAMP-dependent protein kinase, or IκB kinases (Li et al., 2011; Ito et al., 2007; Dzamko et al., 2012; Chia et al., 2014), while the involvement of protein phosphatases in the regulation of LRRK2 phosphorylation and function has not been extensively explored. Our previous study revealed that the protein phosphatase 1 (PP1) catalytic subunit PPP1CA can regulate S935-LRRK2 phosphorylation levels (Lobbestael et al., 2013), although, precise regulatory subunits are not yet known. Indeed, PP1 functions solely as a multimeric enzyme (a.k.a. holoenzyme) consisting of a catalytic and a regulatory subunit, and does not function as free monomers in eukaryotic cells (Virshup and Shenolikar, 2009). Besides the regulation of LRRK2 by PP1, other phosphatases have been reported in relation to LRRK2 as interactors (Liu et al., 2011; Athanasopoulos et al., 2016) or genes whose expression is regulated by LRRK2 (Häbig et al., 2008). For instance, a proteomics screen for interactors of the LRRK2 ROC domain identified the PP2A scaffolding subunit (PPP2R1A) as an interactor of LRRK2 (Athanasopoulos et al., 2016). Subsequent testing reported interaction of the PP2A catalytic subunits (PPP2CA and PPP2CB) with LRRK2 ROC domain and full length LRRK2 (Athanasopoulos et al., 2016). In addition, short hairpin RNA mediated knockdown of PPP2CA/B alleviated toxicity as measured by nuclear fragmentation in cortical neurons from LRRK2 G2019S overexpressing mice and had no effect in neurons from normal mice, specifically suggesting a role for PP2A in LRRK2 mediated toxicity (Athanasopoulos et al., 2016). Also, recent work showed that the Drosophila homologs of PP2A subunits are genetic modifiers of LRRK2-induced toxicity in Drosophila (Sim et al., 2020). Despite these studies linking LRRK2 and PP2A, it remains unclear whether and how PP2A contributes to the regulation of LRRK2 phosphorylation and if so, which PP2A regulatory subunit would be involved (Marchand et al., 2020). Indeed, PP2A, like PP1, functions as a multimeric holoenzyme complex, formed by the association of a catalytic subunit with a regulatory subunit as well as a scaffolding subunit, allowing up to 100 possible combinations of assembled holoenzymes (Janssens et al., 2008; Kiely and Kiely, 2015). Therefore, when studying dephosphorylation by phosphatase holoenzymes it is crucial to decipher not only the catalytic subunit but also the regulatory subunit involved. Finally, as a broad survey of phosphatases and their ability to regulate LRRK2 phosphorylation is still lacking, it cannot be excluded that yet other phosphatases may contribute to LRRK2 phosphoregulation.

Hence, in order to identify additional LRRK2 phosphorylation regulators, we performed a phosphatome-wide reverse genetics screen. The reverse genetics approach has previously successfully been employed to identify the components of phosphatase holoenzymes (Schmitz et al., 2010). Here the findings from our primary screen were confirmed in secondary screens and extensively characterized by using a combination of different models and techniques. Our results both confirmed a role for PP1 and revealed a role for a specific PP2A holoenzyme, denoted PPP2CA:PPPR2RA/B/C/D, in LRRK2 phosphoregulation.

2. Materials and methods

2.1. Constructs and vectors

2.1.1. LRRK2 lentiviral expression constructs

3xFLAG-LRRK2 and eGFP-LRRK2 expression in eukaryotic cells was obtained by lentiviral (LV) vector transduction using the transfer plasmids pCHMWS-3xFLAG-LRRK2 (Lobbestael et al., 2013; Daniëls et al., 2011), pCHMWS-3xFLAG-LRRK2-ires-hygromycin (Vancraenenbroeck et al., 2014) and pLV-CSJ-eGFP-LRRK2.

2.1.2. Phosphatase knockdown constructs

For short hairpin mediated gene knockdown, LV transfer plasmids encoding a miRNA embedded short hairpin sequence (pLV-miR)

directed against the different phosphatase hits were generated as described previously (Reyniers et al., 2014). These knockdown constructs co-express eGFP as well as a zeocin selection marker. Short hairpin sequences cloned are given in Supplementary Table 2. Controls for the knockdown vectors included empty vector control as well as vectors encoding short hairpin sequences targeting firefly luciferase (FLuc) (Osório et al., 2014).

2.1.3. Phosphatase and LRRK2 expression constructs

Constructs were prepared using the Invitrogen Gateway technology. In brief, PCR primers with incorporated attB sites were used to amplify the coding regions of human phosphatase subunits from the plasmids described in (see Supplementary Table 3). PPP1R3D and PPP1R3F were gene synthesized, with attB sites on either end. Construct pcDNA5–Frt–GFP LRRK2 was provided by Dr. Dario Alessi (MRC-PPU, University of Dundee, U.K.) and served as template to generate a human LRRK2 PCR fragment flanked by attB sites. All reading frames were open at the 5′ end. These fragments served as substrates in Gateway BP recombination reactions with donor vector pDONR221 to generate entry clones. Errors leading to amino acid exchanges were corrected using the GeneArt site-directed mutagenesis system from Invitrogen. Expression clones with 5' FLAG, HA or mCherry tags were then created in Gateway LR recombination reactions between the entry clones and destination vectors which were based on the pcDNA5/FRT/TO vector and generated using the Gateway vector conversion system from Invitrogen.

2.1.4. CRISPR/dCas9 LV constructs

LVs used for this study were an in-house designed pLenti-gRNA-J1, containing a gRNA expressed under control of a H1 promoter and containing an hygromycin selection marker. The transcription start site (TSS) was identified using the FANTOM5/CAGE promoter atlas (Radzisheuskaya et al., 2016; Forrest et al., 2014). The sgRNA was designed to target the DNA region from −200 to 100 bp relative to the TSS of the candidate PPP2R2A gene, using the web tool (http://crispr.mit.edu/) to minimize the off-target effect (Hsu et al., 2014). The sequences used in this study were as follows:

PPP2R2A 5′-GACTACGACAGCGACGGCGGCGG-3′
sgRNA neg 5′-GGAGACGAAGCTTAAACGTCTCT-3′

2.2. Chemicals and antibodies

The following LRRK2 inhibitors were used: LRRK2-IN1 (Deng et al., 2011), HG-10-102-01 (Choi et al., 2012), PF-06447475 (Henderson et al., 2015), GNE1023 (Sheng et al., 2012), CZC-25146 (Ramsden et al., 2011), MLi-2 (Fell et al., 2015; Scott et al., 2017). The rationale behind the choice of these inhibitors is as follows: at the time the siRNA screen was performed, LRRK2-IN1 was the inhibitor which had most robustly been demonstrated to induce LRRK2 dephosphorylation and was also the inhibitor we used in our PP1 study (Lobbestael et al., 2013). For the steps validating the hits from the siRNA screen, it was important to include additional compounds of varying chemical classes and with higher potency and selectivity for LRRK2. Indeed, in our previous study, we showed that there is a good correlation between compounds potency to inhibit LRRK2 kinase activity and potency to induce dephosphorylation of the S935 site (Vancraenenbroeck et al., 2014). The additional inhibitors used were therefore selected based on the progressive availability of compounds with better potency and selectivity than LRRK2-IN1.

Mouse anti-GFP (mixture of clones 7.1 and 13.1) and rat anti-HA (3F10) antibodies were from Roche. Rabbit anti-GFP antibody was from Life Technologies. Mouse anti-FLAG (M2), anti-β-tubulin (TUB 2.1), anti-vinculin (hVIN-1) and rabbit anti-FLAG antibodies were from Sigma-Aldrich. Mouse anti-α-actin (AC-15) antibodies were from Sigma-Aldrich and Abcam. Mouse anti-ubiquitin (P4D1) and rabbit antibodies against GFP (D5.1), pan-actin (D18C11), PPP2R1A/B (81G5), PPP2R2A/B/C/D (100C1 and 4953), and PPP2CA/B (52F8) were from Cell Signaling Technology. Mouse anti-PPP2R2A/B/C/D (2G9) antibody was from Thermo Fisher Scientific. Mouse anti-PPP1CA (E-9) antibody was from Santa Cruz Biotechnology. Mouse anti-LRRK2 (N241A/34) antibody was from NeuroMab. Rabbit anti-pS910-LRRK2 (UDD1), anti-pS935-LRRK2 (UDD2), anti-pS955-LRRK2 (MJF-R11), anti-pS973-LRRK2 (MJF-R12), and anti-DARPP32 (EP720Y) antibodies were from Abcam. Secondary antibodies for immunoblotting were from LI-COR Biosciences (IRDye 680RD and 800CW conjugates) and Invitrogen (horseradish peroxidase conjugates). Secondary antibodies for immunofluorescence were from Molecular Probes (Alexa Fluor conjugates).

2.3. Cell culture and transfection

Tissue culture reagents were from Thermo Fisher Scientific or Life Technologies. Human embryonic kidney (HEK)-293 T or HEK-293 cells and SH-SY5Y neuroblastoma cells were maintained in Dulbecco's modified Eagle's medium supplemented with 8–15% fetal bovine serum, 2 mM L-glutamine, and antibiotic/antimycotic solution at 37 °C in a humidified atmosphere containing 5% CO2.

The Flp-In T-REx system was from Invitrogen and stable T-Rex 293 cell lines were generated as per manufacturer instructions by selection with 10–15 μg/ml blasticidin and 100 μg/ml hygromycin B. T-REx cultures were induced to express the indicated protein by inclusion of 1 μg/ml doxycycline in the culture medium for 24 h.

Transfections were performed 8–24 h after seeding with linear polyethylenimine (PEI; Polysciences), Lipofectamine 3000 (Invitrogen) or Fugene 6 (Promega) according to the manufacturer's instructions. When co-expressing multiple plasmids, such as co-expression of catalytic and regulatory phosphatase subunits, molar ratios were respected via transfection of equimolar quantities of the respective plasmids. All cultures were tested and mycoplasma-free.

2.4. Lentiviral vector (LV) production and cellular transduction

LVs encoding human 3xFLAG-LRRK2 under control of the cytomegalovirus (CMV) promoter and co-expressing a hygromycin selection marker via an internal ribosomal entry site element and LVs encoding short hairpins and CRISPR-dCas9 constructs were prepared and used for cellular transduction, essentially as previously described (Vancraenenbroeck et al., 2014; Reyniers et al., 2014; Lobbestael et al., 2010; Civiero et al., 2012; Taymans et al., 2013). In brief, after seeding HEK-293 T cells in a 10-cm dish, we performed a triple transient transfection with the respective transfer plasmids, a packaging plasmid and an envelope plasmid. The medium was replaced after 24 h. Cell supernatant containing lentiviral vectors was collected on day 3 post-transfection, filtered through a 0.45 μm pore size filter (Merck-Millipore) and concentrated using an Amicon Ultra Centrifugal Filter Unit (Sigma).

Expression of LRRK2, dCas9-KRAB, short hairpin constructs or gRNA constructs in HEK-293 T and SH-SY5Y cells was obtained by transduction with LVs generated as described above. For transduction in cell culture, 20,000–50,000 HEK-293 T or 50,000–100,000 SH-SY5Y cells were plated in a 24-well plate. Vector was applied to the cells for 2 days. In the event of selection with an antibiotic, the following concentrations were used: 200 μg/ml hygromycin, 1 μg/ml puromycin and 100 μg/ml zeocin. For conditions with low expression, this transduction procedure was repeated up to two times with the same cells to obtain up to triple transduced cells. Following transduction, cells were lysed for Western blot analysis and/or expanded for use in experiments.

2.5. RNAi screening procedure

Phosphatome-wide siRNA screen was performed using the Silencer® Select Human Phosphatase siRNA Library (Thermo Fisher) directed against 298 phosphatases, including both catalytic and regulatory phosphatase subunits with three siRNA sequences per target. siRNAs were transfected in 96-well plates into U2OS cells expressing GFP-

LRRK2 via transduction with a baculoviral vector (BacMam, Thermo Fisher). Following siRNA treatment, LRRK2 pS935 levels were measured using a FRET signal derived from energy transfer occurring between the GFP tag of LRRK2 and a terbium-marked anti-pS935-LRRK2 antibody (TR- FRET LanthaScreen assay mentioned below). Each plate contained several controls, including wells treated with LRRK2-IN1 (1 μM for 1 h) as a dephosphorylation control (Deng et al., 2011) and wells treated with siRNA directed against LRRK2 or GFP (positive knockdown controls), as well as wells without siRNA or wells treated with non-targeting siRNA control (negative knockdown controls). siRNA screening was performed in quadruplicate in 384-well plates. Only those plates that showed no significant changes between the basal condition and negative knockdown control as well as significant changes between the basal condition and positive knockdown control were taken into account in the analysis. Changes in pS935-LRRK2 levels for a given phosphatase are calculated as a percentage relative to the change observed between the LRRK2 siRNA transfected cells and the non-transfected control. Primary selection of the hits was based on conditions effecting the biggest changes in LRRK2 phosphorylation and hits with minimum 30% change, corresponding to more than three times the variance of the measure on the control condition.

2.6. TR- FRET LanthaScreen cellular assay for LRRK2 pS935

LanthaScreen pS935 assays were performed essentially as described previously (Hermanson et al., 2012). In brief, U2OS cells were transduced with BacMam LRRK2-GFP expressing baculoviral vector (Thermo Fisher) overnight. Cells were replated at 10,000 cells per well in 384 well plates. The cells were either left untreated or treated with siRNA (see above) or 1 μM LRRK2-IN1 (for 60 min). Cells were directly lysed in the presence of terbium-labeled pS935 antibody and after 3 h incubation, TR-FRET ratios for Tb and GFP were read on a Perkin Elmer EnVision plate reader.

2.7. Secondary RNAi screening using LV vector-mediated knockdown

For phosphatase/phosphatase regulators selected from the primary RNAi screen, pLV_miR knockdown LVs were generated as described above. Screening was performed by transduction of HEK-293 T cells stably expressing 3xFLAG-LRRK2 as previously described (Reyniers et al., 2014) with phosphatase targeting pLV_miR LVs and lysates were tested for changes in pS935-LRRK2 levels via dot blot at 72 h post-transduction (Vancraenenbroeck et al., 2014). Transduction conditions in 96-well plates were such that at least 85% of cells were transduced as verified by flow cytometry analysis using the coexpressed eGFP marker at 72 h post-transduction. In the event of pharmacological treatment of transduced cells, pharmacological agents were diluted in pre-warmed culture medium to the concentration and applied for the time indicated in the results section. Cells were rinsed in phosphate-buffered saline (PBS) and lysed in lysis buffer [20 mM Tris-HCl pH 7.5, 150 mM NaCl, 1 mM EDTA, 0.5% Tween-20 or 1% Triton X-100, protease inhibitor cocktail and phosphatase inhibitor cocktail (Roche)]. Lysates were spotted on hydrated polyvinylidene fluoride (PVDF) membranes, and LRRK2 phospho-Ser935 levels as well as total LRRK2 levels were sequentially determined by immunoblot analysis. Densitometric analysis of the immunoreactive spots was performed using Aida analyzer v1.0 (Raytest). Phosphorylation levels were determined as the ratio of phospho-Ser935-LRRK2 to total LRRK2, normalized to values measured for the FLuc short hairpin negative control.

2.8. Expression and purification of recombinant phosphatase subunits and LRRK2

For in vitro experiments, heterotrimeric PP2A holoenzymes (consisting of recombinant FLAG-tagged PPP2R2D and endogenous PPP2R1A/B and PPP2CA/B subunits) and FLAG-tagged CDC25C were purified according to Adams and Wadzinski (Adams and Wadzinski, 2007). In brief, T-REx 293 cells were grown in 15-cm dishes for 24 h, and treated with 1 μg/ml doxycycline to induce overexpression of the FLAG-tagged phosphatases subunits. 48 h later, cells were rinsed with cold PBS, lysed in 1.2 ml lysis buffer (20 mM Tris-HCl pH 7.4, 3 mM EDTA, 3 mM EGTA, 150 mM NaCl, 0.1% Nonidet P-40, and protease inhibitors), and centrifuged at 15,000*g* for 15 min. Cleared supernatants from two dishes were combined and rotated end-over-end with anti-FLAG M2 affinity gel (Sigma-Aldrich) for 1 h at 4 °C. Beads were then washed three times with lysis buffer and once with storage buffer (PP2A: 25 mM Tris-HCl pH 7.4, 1 mM EDTA, 1 mM EGTA, 1 mM DTT, 250 μg/ml BSA; CDC25: 50 mM Tris-HCl pH 7.4, 100 μM EDTA, 250 μM DTT, 150 mM NaCl). Phosphatases were eluted from the beads with 100 μg/ml of 3xFLAG peptide (Sigma-Aldrich) in storage buffer by rotating for 30 min at 4 °C. Protein solutions were supplemented with 50% (PP2A) or 25% (CDC25) glycerol for storage at −20 °C. Catalytic subunits were quantitated by silver stain analysis, with BSA as a standard. PP2A activity was tested using the EnzChek phosphatase assay kit from Molecular Probes (6,8-difluoro-4-methylumbelliferyl phosphate as substrate). CDC25 activity was assayed with the Biomol Green reagent from Enzo Life Sciences (3-*O*-methylfluorescein phosphate as substrate).

For *Xenopus* oocyte microinjection experiments, FLAG-tagged proteins were purified essentially as described previously (Civiero et al., 2012). HEK-293 T cells were cultured in 15-cm dishes and transfected at 70–80% confluence with 30 μg of FLAG-tagged LRRK2 or FLAG-tagged phosphatases subunits constructs using linear PEI (Polysciences). Lysates were made from cells 48 h after transfection in 500 μl of lysis buffer [20 mM Tris-HCl pH 7.5, 150 mM NaCl, 1 mM EDTA, 1% Triton, 10% glycerol including protease and phosphatase inhibitor cocktail (Thermo Fisher Scientific)] for 30 min at 4 °C on a rotary wheel followed by clarification of extracts by centrifugation at 14,000 *g* for 10 min at 4 °C. Supernatant was then incubated for 2 h with constant rocking at 4 °C with 40 μl of anti-FLAG M2-agarose per 0.5 ml of lysate. Beads were then washed four times in wash buffer [25 mM Tris-HCl pH 7.5, 400 mM NaCl, 1% Triton]. Proteins with beads were washed twice in elution buffer prior to elution for 15 min at 4 °C with constant rocking with elution buffer containing 1 mM DTT and 100 μg/ml of 3xFLAG peptide.

2.9. In vitro dephosphorylation assays

Phosphatase assays were set up in a total volume of 20 μl with 5 nM recombinant full-length LRRK2 (Invitrogen) and 5 nM purified phosphatase in reaction buffer (PP2A: 50 mM Tris-HCl pH 7.4, 1 mM MnCl2, 1 mM DTT, 0.1% BSA; CDC25: 50 mM Tris-HCl pH 7.4, 50 mM NaCl, 2 mM DTT), in the presence or absence of okadaic acid (LC Laboratories). Reactions were incubated for 30 min at 30 °C (PP2A) or 37 °C (CDC25), then terminated by the addition of 4xLDS sample buffer (Invitrogen) and boiling for 5 min.

2.10. Cell lysis, immunoprecipitation, and Western blotting

Cell lysates were prepared by washing with cold PBS and lysing in situ with lysis buffer A (50 mM Tris-HCl pH 7.4, 1 mM EDTA, 1 mM EGTA, 270 mM sucrose, 1% Nonidet P-40 and protease inhibitors) or lysis buffer B (20 mM Tris-HCl pH 7.5, 150 mM NaCl, 1 mM EDTA, 1% Triton, 10% glycerol, supplemented with protease and phosphatase inhibitors) on ice. To study ubiquitination, lysis buffer was supplemented with 10 mM N-ethylmaleimide (NEM). Lysates were subsequently centrifuged at 15,000 *g* for 15 min at 4 °C to pellet cell debris. Protein content of cell lysates was determined using the bicinchoninic acid (BCA) protein determination assay (Pierce Biotechnology) or the Bradford method (Thermo Scientific) with bovine serum albumin (BSA) as the standard. After addition of LDS sample buffer and boiling, 10–20 μg cell lysates were resolved by electrophoresis on NuPAGE 3–8% Tris-Acetate gradient gels, 4–12% Bis-Tris gradient gels, 4–12% Tris-Glycine gradient gels or 12.5% SDS gels (LifeTechnologies). Separated

proteins were transferred to PVDF (Bio-Rad) or nitrocellulose (Amersham) membranes, and non-specific binding sites were blocked for 30 min in Tris-buffered saline containing 0.1% Tween-20 (TBS-T) and 5% non-fat milk or 5% BSA. After overnight incubation at 4 °C with the appropriate antibodies, blots were washed three times with TBS-T. After incubation with the secondary antibodies, blots were washed again. Bands were visualized using enhanced chemiluminescence (Amersham Pharmacia Biotech) or LI-COR dual probes. Densitometric analysis of the bands on the blot autoradiograms were performed using Aida analyzer v1.0 (Raytest), image analyzer ImageQuant 600 (GE Healthcare Bio-Sciences), or a LI-COR Odyssey infrared imaging system.

For immunoprecipitations, 500 µl of lysates was incubated end-over-end with GFP-Trap_A beads (ChromoTek) for 1 h at 4 °C. Beads were then washed twice with lysis buffer A supplemented with 300 mM NaCl, and twice with wash buffer (50 mM Tris-HCl pH 7.4, 0.1 mM EGTA, 270 mM sucrose, 50 mM NaCl). Immune complexes were incubated at 70 °C for 10 min in LDS sample buffer, and passed through a Spin-X column (Corning) to separate the eluates from the beads, then boiled before loading on gels.

2.11. Immunofluorescence and determination of degree of co-localization

Transfected HEK-293 T cells cultured on poly-D-lysine coated coverslips were fixed with 4% paraformaldehyde for 15 min at room temperature, followed by three wash steps with PBS, permeabilization with 0.1% Triton X-100 for 5 min, and were then blocked for 30 min at room temperature using blocking solution (0.5% BSA in PBS). The coverslips were incubated overnight with primary antibodies (anti-FLAG M2 and anti-GFP) in PBS. After three washes with PBS for 5 min, the cells were incubated for 1 h with secondary antibody (Alexa Fluor conjugates) and washed three times for 5 min with PBS. The coverslips were mounted on a microscope slide with UltraCruz hard-set mounting medium (Santa Cruz Biotechnology). Capture of confocal images was performed using a laser scanning confocal microscope (LSM 710, Zeiss) with a 63× oil-immersion objective. Counts were based on 10 randomly taken confocal images. Pearson's correlation coefficient (PCC, or colocalization coefficient) value was given by the JACoP plug-in using ImageJ software for each individual cell.

2.12. Videomicroscopy

HEK-293 T cells were plated on 35 mm glass-bottom culture µ-dishes (Biovalley) and transfected with GFP-LRRK2 and mCherry-PPP1CA, mCherry-PPP1CB, mCherry-PPP1CC, mCherry-PPP2CA or mCherry-PPP2CB. Capture of confocal time-lapse images was performed using a Zeiss Observer Z1 spinning disk confocal microscope (Bio Imaging Center Lille) with a 63× oil-immersion objective at one frame per minute for 60 min with recordings starting when the LRRK2 inhibitor PF-06447475 compound was added to the medium. Confocal microscope settings were kept constant for all scans in each experiment. The analysis of the PCC was performed using ImageJ software and the JACoP plug-in. PCC was measured for each individual cell by hand-drawing a region of interest (ROI) over the image. The co-loc index is the PCC normalized to 1 at the zero time point (i.e. the moment at which either DMSO or compound are added) and all other values at other time points are given relative to this value within a given run. From the graph of the co-loc index relative to time, an area under the curve is then calculated as a cumulated value of the areas under the curve per 5 min intervals.

2.13. Proximity ligation assay

Proximity ligation assays (PLA) were performed on formaldehyde-fixed cells as in immunocytochemistry experiments. After permeabilization for 5 min with PBS-T (PBS supplemented with 0.1% Triton X-100), cells were blocked with Duolink blocking solution for 30 min at 37 °C. Immediately after blocking, the cells were incubated with indicated primary antibodies in the Duolink antibody diluent for 1 h at room temperature. The cells were washed twice with Duolink wash buffer A for 5 min before the incubation of the PLUS and MINUS PLA probes. The cells were incubated with PLA probes for 1 h at 37 °C, followed by two times washing with wash buffer A for 5 min. The cells were then incubated with pre-mixed Ligation-Ligase solution at 37 °C for 30 min. After two times washing with wash buffer A for 2 min, the cells were incubated with pre-mixed Amplification-Polymerase solution for 90 min, at 37 °C. Finally, the cells were washed twice with Duolink wash buffer B for 10 min, followed by 0.01× wash buffer B for 1 min. The coverslips were dried in the dark and mounted with UltraCruz hard-set mounting medium. Images were quantitated in ImageJ using the Cell Counter plugin.

2.14. Assessment of LRRK2 phosphorylation in phosphatase-injected Xenopus laevis oocytes

Oocyte micromanipulation and microinjection of purified proteins were performed as described previously (de Broucker et al., 2015). Fifty nanoliters of purified 3xFLAG-LRRK2 protein was injected first followed after 30 min by the microinjection of fifty nanoliters of protein phosphatases (either catalytic subunit alone or with the regulatory subunit) representing time point 0 of the experiment. Oocytes were collected at 30 min, 1, 2 and 4 h post-injection of PP2A subunits. Ten oocytes were collected and assayed per experimental replicate, all experimental conditions were performed in triplicates. Oocytes were homogenized in lysis buffer (100 µl/10 oocytes) containing 25 mM MOPS pH 7.2, 60 mM β-glycerophosphate, 15 mM paranitrophenyl phosphate, 15 mM EDTA, 15 mM MgCl2, 2 mM DTT, 1 mM orthosodium vanadate, 1 mM NaF, 1 mM phenylphosphate, 10 µg/ml leupeptin, 10 µg/ml aprotinin, 10 µg/ml soybean trypsin inhibitor, 10 µM benzamidine, and subsequently centrifuged at 10,000 *g* for 15 min at 4 °C. Lysate from ten oocytes was analyzed by immunoblotting. LRRK2 (recombinant protein; Life Technologies) was used as an internal control. Densitometric analysis of the immunoreactivity bands was performed using ImageJ software.

2.15. Measurement of PP2A subunit expression levels in post-mortem brain and in patient derived lymphoblastoid cells

For post-mortem brain samples, patient information as well as protein extraction and immunoblotting procedures were described in reference (Dzamko et al., 2017). Experiments using human brain tissue lysates were approved by the University of NSW Human Research Ethics Advisory (#HC14046). For the patient derived lymphoblastoid samples, patient information, ethical committee approval as well as protein extraction and immunoblotting procedures were described in reference (Fernández et al., 2019).

2.16. Statistics

All data presented in this study were either averages or representative data from at least three independent experiments. The number of independent experiments and sample size are indicated in the figure legends. Statistical analyses were conducted using the GraphPad Prism 7 software (GraphPad Software). Statistical analyses conducted in specific experiments are indicated in the figure legends. In brief, comparisons of a test group with a control group were conducted with Mann-Whitney *U* test or *t*-test, two-tailed by default or one-tailed in the event a hypothesis exists for the direction of change. Time course experiments were tested using 2-way ANOVA, using time and experimental conditions as the 2 factors, followed by Bonferroni *post-hoc* test to compare the effects of test groups against control group condition for each time point. Statistical significance in the subcellular localization scoring experiments was tested by one-way ANOVA with *post-hoc* Fisher's LSD test for multiple comparisons. Data are expressed as mean ± s.e.m. Significance levels in the figures are denoted as ns, *, **, ***, **** corresponding to not

significant ($P > 0.05$), $P < 0.05$; $P < 0.01$; $P < 0.001$ and $P < 0.0001$, respectively.

3. Results

3.1. Phosphatome-wide reverse genetics screen for regulators of Ser935-LRRK2 phosphorylation

In order to identify phosphatases involved in the dephosphorylation of the LRRK2 phosphosites clustered in the interdomain region between the ankyrin repeat (ANK) domain and leucine-rich repeat (LRR) domain (S910/S935/S955/S973; Fig. 1A), we performed a phosphatome-wide RNAi screen using siRNAs directed against 298 phosphatases and phosphatase regulatory proteins in LRRK2 expressing U2OS cells (Fig. 1B). As readout, we chose a previously developed high throughput method using time-resolved FRET that detects pS935-LRRK2 levels in cellular lysates (Hermanson et al., 2012). Assay performance was confirmed on each plate using multiple controls, including reduced pS935-LRRK2 following pharmacological LRRK2 kinase inhibition as well as following siRNA knockdown of LRRK2. In addition, we observed no significant difference in pS935-LRRK2 levels between untransfected cells and cells transfected with a non-targeting negative control siRNA.

A graphic overview of the effects of siRNA-mediated knockdown of individual phosphatases on pS935-LRRK2 is given (Fig. 1C). Values of pS935-LRRK2 levels averaged over the three siRNAs tested per phosphatase/phosphatase regulator are ranked from lowest to highest and range from −55% to +55% relative to the no knockdown control. At a macro level, it is apparent that the majority of the siRNAs lead to an increase in LRRK2 phosphorylation levels. From the 298 different phosphatases and phosphatase regulators tested in this primary screen (Fig. 1C and Supplementary Table 1), we selected 39 candidate phosphatases/phosphatase regulators for confirmation in a secondary screening. This selection was based firstly on the amplitude of the change in LRRK2 pS935 phosphorylation effected by the phosphatases/phosphatase regulator knockdown. The most important changes were categorized under PP1-related, PP2A-related, tyrosine phosphatases, as well as dual specificity and other phosphatases. Some additional phosphatases were included for further testing based on their close homology to positive hits. For instance, PPP1CA and PPP1CC were included in the list despite a modest effect of the knockdown because of their close homology with PPP1CB, one of the top hits.

3.2. Secondary screen via phosphatase subunit knockdown

For each of the 39 selected hits, two knockdown constructs per hit were cloned in LV transfer plasmids encoding a miRNA embedded short hairpin sequence directed against the different phosphatase hits (pLV_miR (Osório et al., 2014), see Supplementary Table 2). LVs for phosphatase/phosphatase regulator knockdown were used to transduce LRRK2 expressing cells both in the presence and the absence of the compound LRRK2-IN1. Although the S935 site and other sites in this phosphosite cluster were demonstrated to be heterologous phosphorylation sites (Chia et al., 2014; Ito et al., 2014), rapid dephosphorylation of these sites can be induced by LRRK2-IN1 (Deng et al., 2011) and in general by most inhibitors of LRRK2 kinase activity (Dzamko et al., 2010; Vancraenenbroeck et al., 2014). As we have shown previously that LRRK2-IN1 mediated S935-LRRK2 dephosphorylation is dependent on phosphatases (Lobbestael et al., 2013), we here combined phosphatase knockdown with LRRK2 inhibitor treatment in order to test candidate LRRK2 phosphatases in dephosphorylation conditions (Fig. 1D-F). The secondary knockdown screen revealed an overall trend to increases in LRRK2 phosphorylation and knockdown hits mostly related to PP2A were confirmed to modulate LRRK2 phosphorylation under these test conditions.

3.3. Secondary screen via overexpression of catalytic and regulatory phosphatase subunits

Prior to selecting hits for in-depth characterization, we decided to also test the effects of phosphatase overexpression on LRRK2 S935 phosphorylation, for the PP1-, PP2A- and CDC-related hits. We tested the activity of reconstituted complexes on LRRK2 in cells, using co-expression (Fig. 2). Of the seven putative PP1 regulatory subunits that scored highly in our screens as potential LRRK2 regulators, we found that the PPP1CA:PPP1R3F complex reproducibly induced LRRK2 dephosphorylation across multiple sites of the S935 cluster (Fig. 2A). We next tested co-expression of catalytic PP2A subunits along with the various regulatory subunits, with the scaffolding subunit being constant at endogenous levels. For the eight different regulatory subunits tested, we found that PPP2R2A/B/C/D and to a lesser extent PPP2R3C induced reductions in LRRK2 phosphorylation (Fig. 2B). We also found that expression of CDC25A/B/C all induced LRRK2 dephosphorylation (Fig. 2C), with CDC25C showing the greatest effect.

3.4. Subcellular co-localization analysis of LRRK2 and phosphatase subunits via fluorescence microscopy and videomicroscopy

Based on the results of the primary screen and secondary screens, we decided to further characterize the PP1, PP2A and CDC related hits.

One way of further confirming candidate LRRK2 phosphatases is to examine their overlap with LRRK2 in subcellular localization. LRRK2 is diffusely located in the cytoplasm under basal conditions. However, after the induction of LRRK2 dephosphorylation by kinase inhibition or in the presence of some LRRK2 clinical mutants, LRRK2 will relocate to discrete filamentous accumulations or punctae. Therefore, we proceeded to test subcellular co-localization of LRRK2 and phosphatases under basal conditions and in conditions of kinase inhibitor induced dephosphorylation. We assessed whether the colocalization between candidate LRRK2 phosphatases and LRRK2 is modulated in conditions of LRRK2 dephosphorylation in HEK-293 T cells co-transfected with FLAG-phosphatases (17 different candidate phosphatases) and GFP-LRRK2 and treated one hour with LRRK2 inhibitor HG-10-102-01 (Choi et al., 2012) or DMSO.

As previously described (Dzamko et al., 2010; Deng et al., 2011; Sheng et al., 2012), GFP-tagged wild-type LRRK2 protein was found in a purely cytosolic localization in the majority of cells (Fig. 3A). Under basal condition, PP1 isoforms colocalized with LRRK2 in the cytoplasm except for PPP1CC, PPP1R3B, PPP1R3F, PPP1R16B and PPP1R8 (Fig. 3A, Supplementary Fig. S1). Most of the PP2A isoforms were primary localized in the nucleus (Fig. 3A, Supplementary Fig. S2). We observed an increased colocalization for LRRK2 with PPP1CC, PPP1R1B and PPP1R3B after one hour treatment with HG-10-102-01 compound (Fig. 3A, B). Interestingly, we observed a significant enhancement of the colocalization between LRRK2 and PPP2CA, PPP2CB, PPP2R2A and PPP2R3C in the cytoplasm of the cells after inhibitor treatment (Fig. 3A, B). We also performed live cell imaging to test PP1 and PP2A recruitment to LRRK2 in conditions of dephosphorylation with the PF-06447475 LRRK2 kinase inhibitor (Henderson et al., 2015) (Fig. 3C, D and Supplementary Fig. S3). In cells co-transfected with mCherry-tagged catalytic subunits and GFP-tagged LRRK2, colocalization of PPP1CA and PPP1CB with LRRK2 was enhanced rapidly after inhibitor addition (Fig. 3C, D and Supplementary Fig. S3A). We also observed an enhanced colocalization between LRRK2 and PPP2CA (Fig. 3C, D) and PPP2CB (Supplementary Fig. S3C) within minutes after application of LRRK2 kinase inhibitor, consistent with the observation in the immunocytochemistry experiment (Fig. 3B).

Dephosphorylation of LRRK2 can be induced either via extrinsic and/or intrinsic factors, respectively kinase inhibitors (Fell et al., 2015) and phosphatase holoenzymes for examples (Fig. 2). The subcellular localization of LRRK2 may be modulated by pharmacological inhibition of LRRK2 kinase activity (Fig. 3C, D). We next thought to examine the

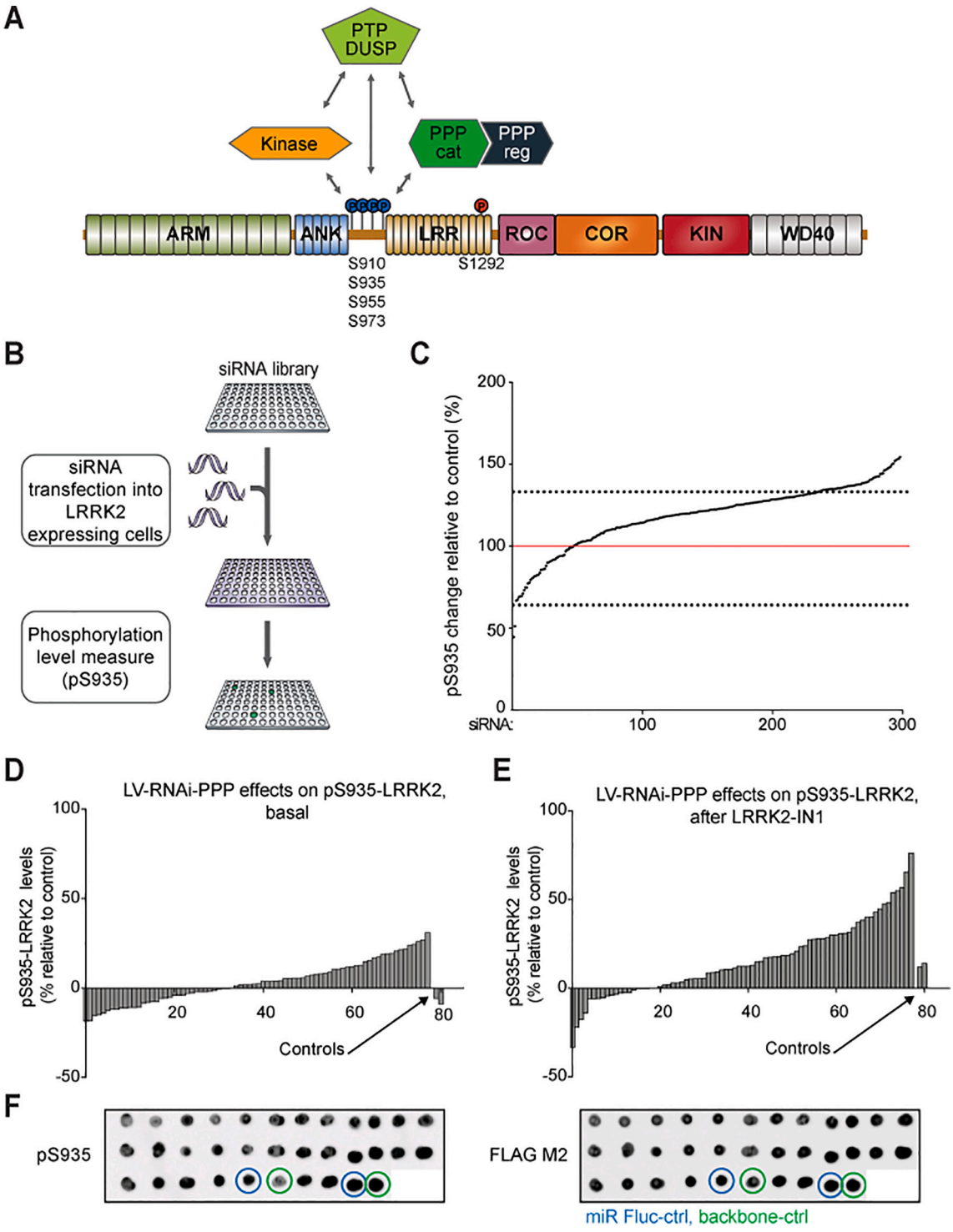

Fig. 1. Identification of candidate phosphatases via reverse genetics with a phosphatome-wide siRNA library and genetic depletion. (A) Schematic representation of LRRK2 domain structure, indicating the relative position of the phosphosites studied. Abbreviations: PPP: phosphoprotein phosphatase (serine/threonine), PTP: protein tyrosine phosphatase, DUSP: dual specificity phosphatase. (B) Schematic approach of the siRNA screen against phosphatases. (C) Changes in LRRK2 S935 phosphorylation induced by siRNA-mediated knockdown of 298 phosphatases and phosphatase regulators are depicted in the diagram, with values relative to control ranked from lowest to highest. Numerical values are given in (Supplementary Table 1). (D, E) Secondary screen of candidate phosphatases via genetic depletion. For the different phosphatase hits, two knockdown constructs per hit were cloned into lentiviral vector (LV) transfer plasmids encoding a miRNA embedded short hairpin sequence. Changes in LRRK2 S935 phosphorylation induced by short hairpin mediated-knockdown of 39 candidate phosphatases compared to negative controls in basal condition (D) and in the presence of LRRK2-IN1 (E). (F) Representative dot blot images from the secondary screen. The left panel shows the detection of the pS935-LRRK2 and the right panel the detection of total LRRK2 using an anti-flag tag antibody on the same dot blot membrane. Circles indicate detection of the samples of the control conditions, including the condition with the negative control short hairpin directed against firefly luciferase (blue circles) and the empty vector backbone control (green circles). See Materials and Methods for more details. (For interpretation of the references to colour in this figure legend, the reader is referred to the web version of this article.)

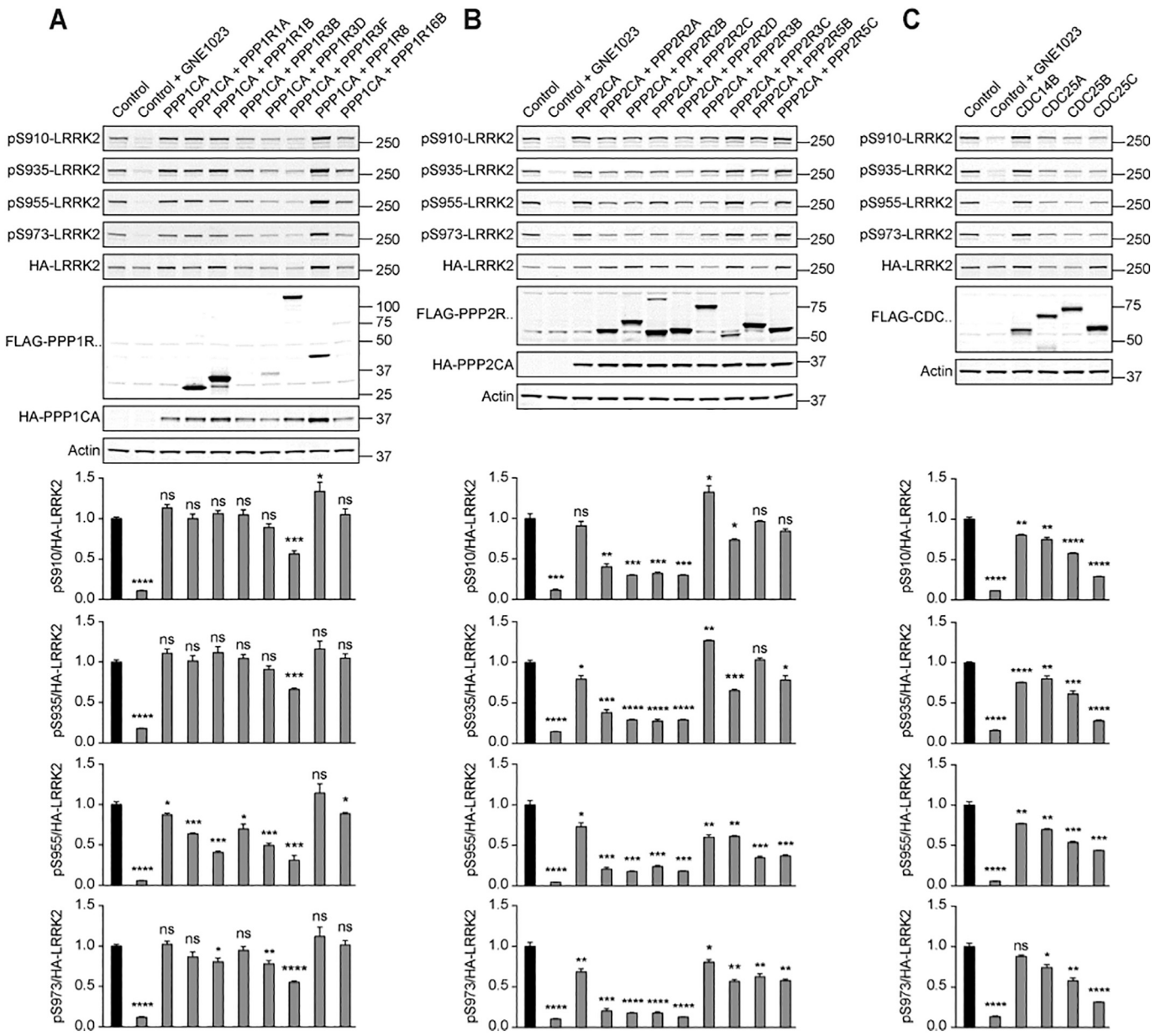

Fig. 2. Secondary screen of candidate LRRK2 phosphatases via overexpression analysis. (A) HEK-293 cells were transiently transfected with cDNAs encoding HA-tagged LRRK2, HA-tagged catalytic PP1 subunits, and FLAG-tagged regulatory PP1 subunits, as indicated. Changes in LRRK2 phosphorylation at S910, S935, S955, and S973 were measured by quantitation of immunoblots. (B) HEK-293 cells were transiently transfected with cDNAs encoding HA-tagged LRRK2, HA-tagged catalytic PP2A subunits, and FLAG-tagged regulatory PP2A subunits, as indicated. (C) HEK-293 cells were transiently transfected with cDNAs encoding HA-tagged LRRK2 and FLAG-tagged CDC14B, CDC25A, CDC25B, or CDC25C. Graphs show mean ± s.e.m. ($n = 3$). Statistical significance tested with two-tailed *t*-test (*$P < 0.05$; **$P < 0.01$; ***$P < 0.001$; ****$P < 0.0001$; ns = not significant).

effect of PP2A phosphatase holoenzymes (Fig. 4A) overexpression on LRRK2 subcellular distribution. To do so, we scored and assigned to one of four phenotypes, namely 1) diffuse localization, 2) filamentous skein-like structures, 3) punctae structure and 4) amorphous: accumulations (Fig. 4B). As shown previously, in control conditions, GFP-tagged wild-type LRRK2 protein was found in a purely cytosolic localization in the majority of cells, 80% of the cells (Fig. 4C). Overexpression of PP2A catalytic subunit alone, PPP2CA or PPP2CB did not affect LRRK2 subcellular localization (Fig. 4C). Interestingly, we observed a significant diminution of LRRK2 diffuse localization after PP2A holoenzyme overexpression, PPP2CA:PPP2R2A (Fig. 4C). We also found that PPP2CB:PPP2R2C holoenzyme increased significantly the percentage of cells presenting LRRK2 filamentous and punctae relocalisation compared to the control condition (Fig. 4C). We confirmed that overexpression of the reconstituted holoenzymes induced LRRK2 dephosphorylation at S935 (Supplementary Fig. S4).

3.5. Analysis of interaction between LRRK2 and phosphatases via proximity ligation assay (PLA)

In our initial study, we found that dephosphorylation of LRRK2 was accompanied by a dynamic recruitment of PP1 to the LRRK2 complex (Lobbestael et al., 2013). In the same study, we did not detect the recruitment of PP2A scaffolding subunit to LRRK2 under dephosphorylation conditions, although we did not test PP2A catalytic and regulatory subunits (Lobbestael et al., 2013). Therefore, besides changes in subcellular localization we wanted to know which candidate phosphatases physically interact with LRRK2 in the cell. We used in situ

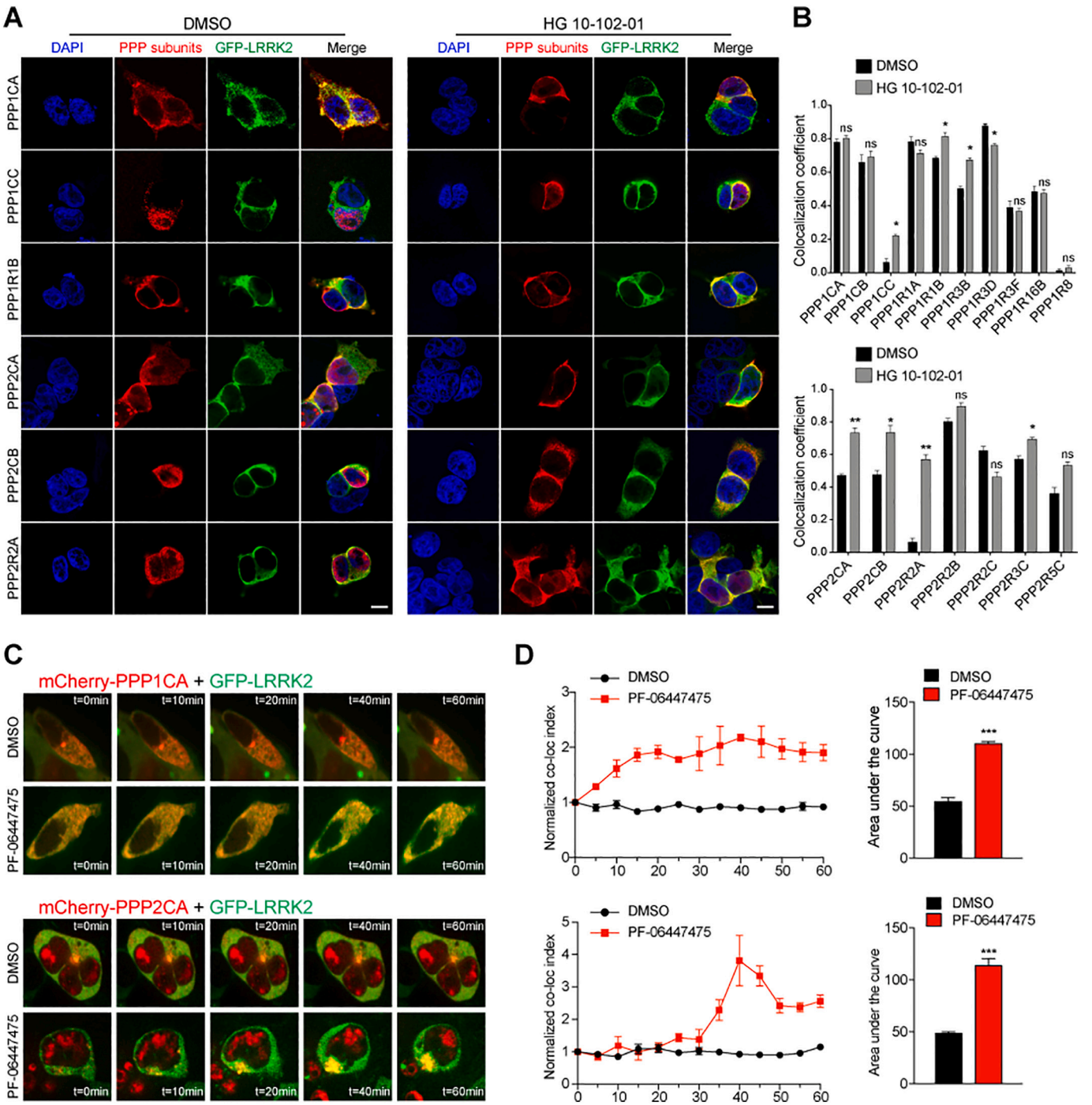

Fig. 3. Pharmacological induction of LRRK2 dephosphorylation results in a recruitment of PP1 and PP2A phosphatases to the LRRK2 compartment. (A) Colocalization assay from transfected HEK-293 T cells treated with DMSO or 1 μM HG-10-102-01 for 1 h. HEK-293 T cells were transfected with FLAG-tagged catalytic and regulatory subunits of protein phosphatases and GFP-tagged LRRK2. Cells were stained with DAPI to visualize nuclei (blue, first column of images) and proteins were detected by immunofluorescence using FLAG for PPP isoforms (red, second column) and eGFP for LRRK2 (green, third column). Merged images are shown in the right-hand panels. Scale bar shown is 10 μm. (B) Quantification of the LRRK2/phosphatases correlation coefficient (Rcoloc) values for PP1 and PP2A isoforms shown in panel (A) and see Supplementary Fig. S1, S2. Data are from three independent co-transfection experiments. Graphs show mean ± s.e.m. Statistical significance tested with Student's *t*-test (*$P < 0.05$; **$P < 0.01$; ns = not significant). (C) Dynamic relocalization of phosphatases with LRRK2 under pharmacological inhibition. Live images of HEK-293 T cells transfected with GFP-tagged LRRK2 and mCherry-tagged PPP1CA or PPP2CA as indicated at distinct time points after adding DMSO or 150 nM PF-06447475. (D) Quantification of the colocalization index between LRRK2 and phosphatases during a period of 60 min and the area under the curve for data shown in (C). Graphs show mean ± s.e.m. ($n = 5$). Statistical significance tested with Student's t-test (***$P < 0.001$). Results of the same experiments performed for PPP1CB, PPP1CC and PPP2CB are given in Supplementary Fig. S3. (For interpretation of the references to colour in this figure legend, the reader is referred to the web version of this article.)

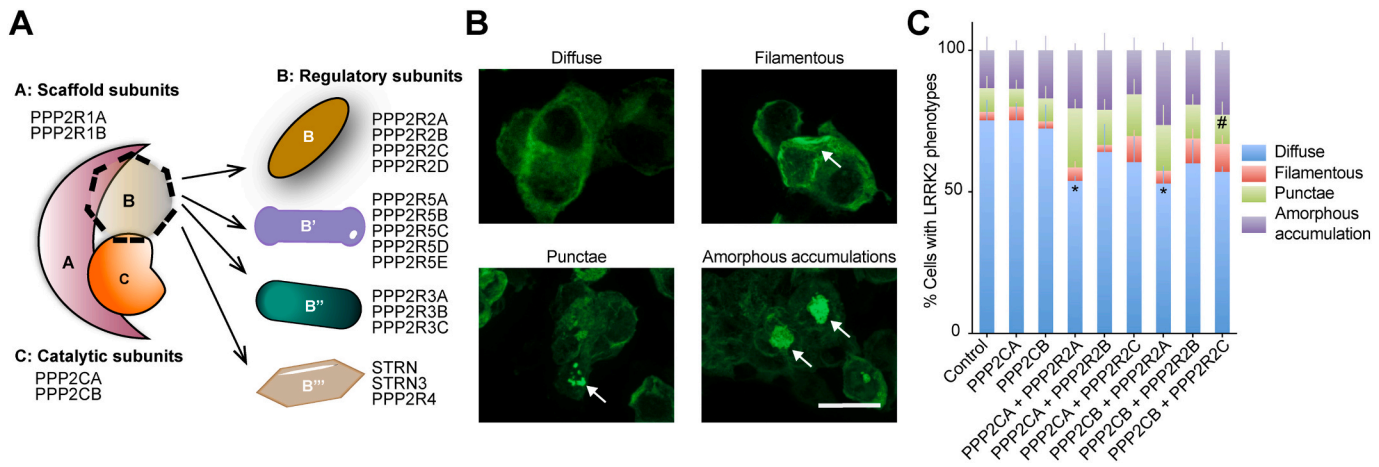

Fig. 4. Effects of PP2A holoenzymes on LRRK2 subcellular localization. (A) Schematic structure of PP2A holoenzyme complex. PP2A is composed of three subunits, a catalytic, a scaffold and a regulatory subunit. The B regulatory subunit is involved in determining substrate specificity and subcellular localization. (B) Representative images of the four LRRK2 phenotypes observed after PP2A overexpression in HEK-293 T cells. Cytoplasmic aggregates of GFP–LRRK2 are indicated with white arrows and are defined as follow, diffuse: purely diffuse localization; filamentous: presence of clear filamentous skein-like structures; punctae: presence of dot-like structure (small and perinuclear); amorphous: accumulation. Scale bar shown is 20 μm. (C) Quantitation of proportion of cells with LRRK2 phenotypes shown in (B). Data are from $n > 40$ cells in four independent co-transfection experiments per construct. Graphs show mean ± s.e.m. Statistical significance tested by one-way ANOVA with *post-hoc* Fisher's LSD test for multiple comparisons ($^{*,\#}P < 0.05$; symbol * denotes significant differences compared to the control for the diffuse phenotypes, symbol $^{\#}$ denotes significant differences compared to the control for both the punctae and filament phenotypes).

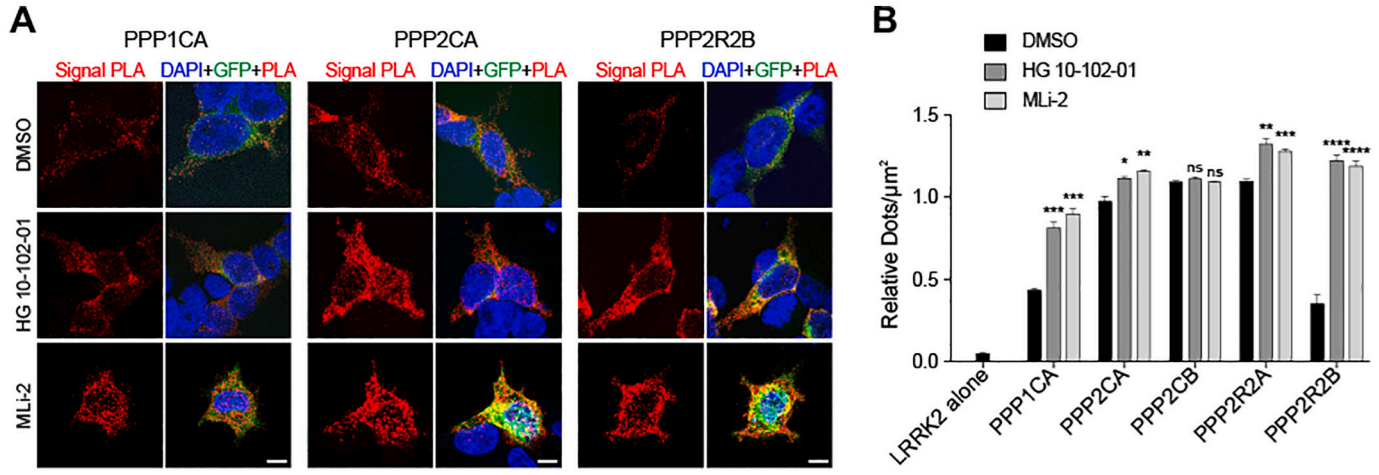

Fig. 5. Enhanced LRRK2 interaction with PP1 and PP2A subunits in the presence of LRRK2 kinase inhibitors. (A) The interaction between phosphatases and LRRK2 was analyzed in HEK-293 T cells in the presence of LRRK2 kinase inhibitors using in situ PLA, as described in the methods section. HEK-293 T cells were transfected with GFP-tagged LRRK2 and FLAG-tagged phosphatases as indicated. At 48 h after transfection, cells were subjected to PLA using primary antibodies against GFP and FLAG. Representative confocal images are shown for cells expressing PPP1CA, PPP2CA or PPP2R2B, either treated with DMSO (control), or with inhibitors HG-10-102-01 (1 μM) or MLi-2 (10 nM) for 1 h. Scale bar shown is 10 μm. (B) PLA signals per cell were quantified using ImageJ software and the Cell Counter plugin, for conditions depicted in panel (A) as well as control and test conditions shown in (see Supplementary Fig. S5). Values are means±s.e.m. of three separate experiments. Statistical significance was tested with Student's *t*-test ($^{*}P < 0.05$; $^{**}P < 0.01$; $^{***}P < 0.001$; $^{****}P < 0.0001$; ns = not significant).

detection of LRRK2-phosphatase holoenzymes by PLA on cells co-expressing FLAG-tagged phosphatases and GFP-LRRK2 and quantified the number of individual ligation amplification signals per cell (Fig. 5A, B and Supplementary Fig. S5). We observed a significant increase of PLA signals after treatment with the LRRK2 dephosphorylation inducers HG-10-102-01 or MLi-2 for PPP1CA, PPP2CA and the two regulatory subunits of PP2A (PPP2R2A and PPP2R2B), but not for PPP2CB (Fig. 5A, B and Supplementary Fig. S5A, B). Control amplifications with GFP-LRRK2 alone yielded no PLA signals (Supplementary Fig. S5B).

3.6. *In vitro dephosphorylation of LRRK2 by PP2A*

An important step in validating candidate LRRK2 phosphatases is to assess the capacity of these to directly dephosphorylate LRRK2 in vitro. We have previously shown that PPP1CA efficiently dephosphorylates LRRK2 in vitro, however we also showed only weak ability of the catalytic subunit of PP2A to dephosphorylate LRRK2 (Lobbestael et al., 2013). The novelty in the present study is that we tested LRRK2 dephosphorylation in the presence of reconstituted heterotrimeric PP2A holoenzymes by isolating regulatory subunits with immunoaffinity chromatography, and co-purifying endogenous scaffolding and catalytic subunits (Supplementary Fig. S6). Full-length recombinant wild type LRRK2 and the G2019S, R1441C and D1994A mutants were dephosphorylated by the PPP2CA/B:PPP2R1A/B:PPP2R2D holoenzyme complex (Fig. 6A). This dephosphorylation was blocked by the PP2A inhibitor okadaic acid (Fig. 6B). These experiments confirmed that LRRK2 ANK-LRR interdomain phosphosites are direct substrates for PP2A. Recombinant CDC25 did not induce LRRK2 dephosphorylation in

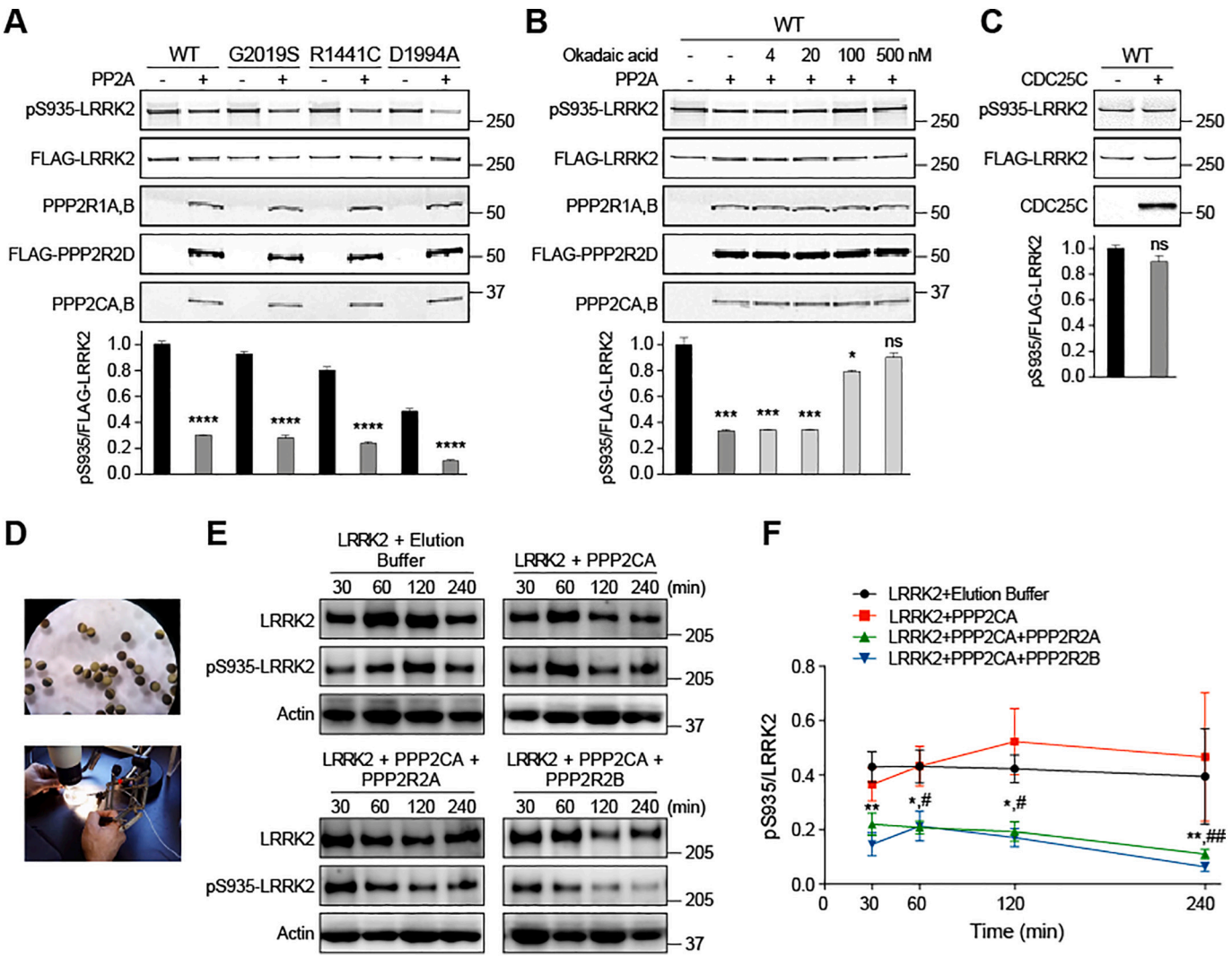

Fig. 6. PP2A directly dephosphorylates LRRK2 in vitro and in Xenopus oocytes. (A) Wild-type and mutant LRRK2 were significantly dephosphorylated at S935 in the presence of purified trimeric PP2A complexes (consisting of recombinant, FLAG-tagged PPP2R2D regulatory subunit and endogenous catalytic and scaffolding subunits). (B) Dephosphorylation of LRRK2 by PP2A was sensitive to okadaic acid. (C) Purified CDC25C had no effect on LRRK2 dephosphorylation. Graphs show mean ± s.e.m. ($n = 3$). Statistical significance tested with two-tailed t-test (*$P < 0.05$; **$P < 0.01$; ***$P < 0.001$; ****$P < 0.0001$; ns = not significant). (D) Experimental overview of microinjection of recombinant phosphoprotein phosphatase complex PPP2CA + PPP2R2A and PPP2CA + PPP2R2B in Xenopus. (E) Effect of phosphatase injection on the overall LRRK2-S935 phosphorylation level. Xenopus oocytes were microinjected first with LRRK2 protein and then with PP2A (catalytic subunit alone or in combination with its regulatory subunits) as indicated. Blots show representative results of three experiments. (F) Quantification of blots shown in (E). Graph shows mean ± s.e.m. Statistical significance tested by 2-way ANOVA with time and phosphatase combination as factors followed by Bonferroni *post-hoc* test to compare the effects of test groups against control group (LRRK2 + elution buffer) condition for each time point (*,#P < 0.05; **,##P < 0.01; ns = not significant; symbols * and # denote significant differences for LRRK2 + PPP2CA:PPP2R2B or LRRK2 + PPP2CA:PPP2R2A groups which show reduced LRRK2 phosphorylation compared to the LRRK2 + elution buffer control group). The experiment was carried out three times from two independent microinjections.

vitro (Fig. 6C), despite being implicated in LRRK2 dephosphorylation in HEK-293 cells (Fig. 2C) indicating an indirect effect on LRRK2 dephosphorylation.

3.7. Assessment of LRRK2 phosphorylation in phosphatase-injected Xenopus laevis oocytes

As further validation by in vitro experiments, we tested reconstituted PP2A holoenzymes in *Xenopus* oocytes that allows testing of recombinant proteins in a cellular environment following direct microinjection (Fig. 6D), thereby circumventing the issue of the large time difference between the phosphorylation changes of LRRK2 occurring in short time frames (<1 h) and the longer times needed to achieve overexpression or knockdown of phosphatases via plasmid or LV constructs (Fig. 6E, F). When we injected PP2A subunits, we found that the catalytic subunit PPP2CA alone did not significantly dephosphorylate LRRK2 compared to the control. Interestingly, when the PP2A holoenzyme was completed with PPP2R2A or PPP2R2B regulatory subunits, we observed a significant and rapid dephosphorylation of LRRK2 compared to both the group injected with PPP2CA alone and the buffer control group (Fig. 6F).

3.8. Validation of LRRK2 phosphatase holoenzymes by modulation of phosphatase subunit expression

In order to investigate whether specific PP2A holoenzymes regulate LRRK2 phosphorylation, we generated SH-SY5Y cells with stable overexpression of LRRK2 and stable combined knock down of the catalytic PPP2CA subunit and regulatory PPP2R2A/B/C subunits. Treatment for 24 h with LRRK2 kinase inhibitor PF-06447475 revealed that reduced levels of PPP2CA and PPP2R2A/B/C can prevent LRRK2

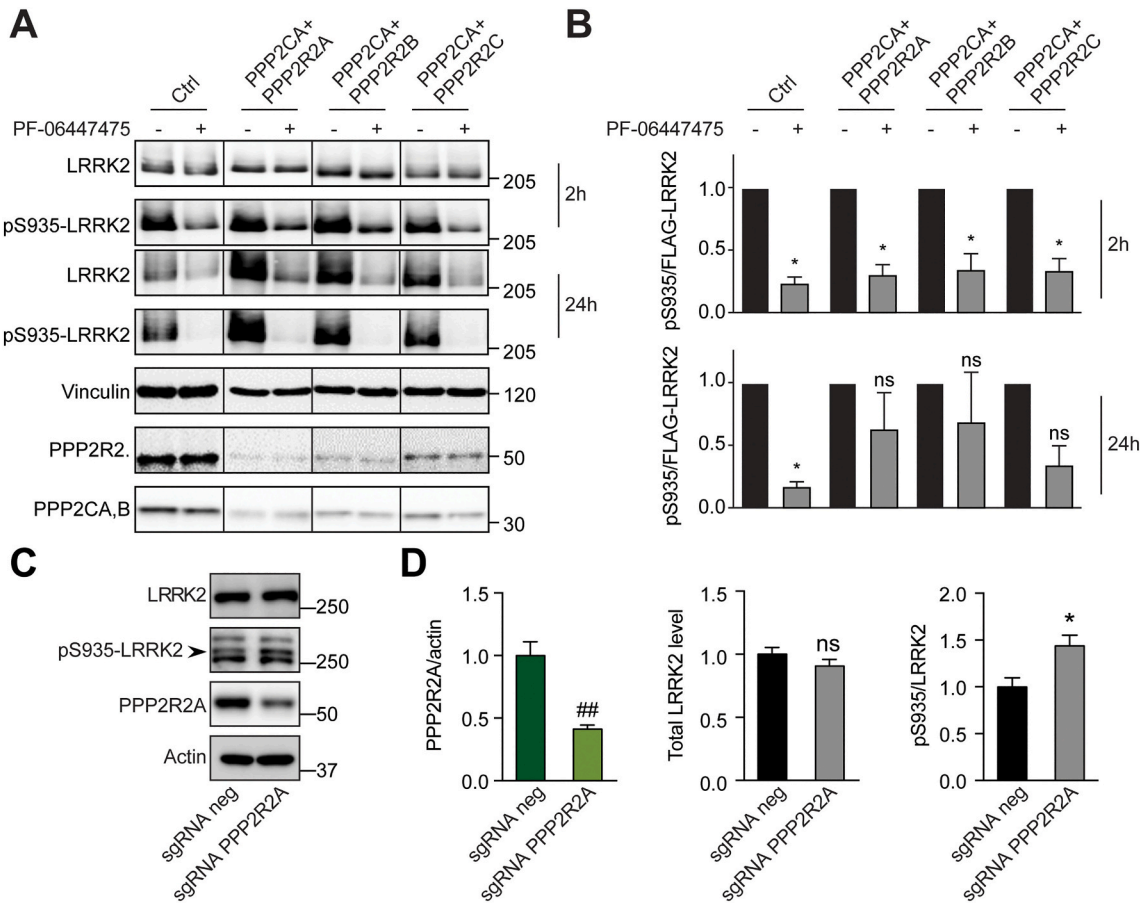

Fig. 7. Effects of modulation of PP2A expression on LRRK2 phosphorylation in SH-SY5Y cells. (A, B) Effect of combined PP2A catalytic and regulatory subunit knockdown on LRRK2 S935 phosphorylation. SH-SY5Y cells with stable expression of LRRK2 and stable combined knock down of PPP2CA and PPP2R2A, were treated with LRRK2 kinase inhibitor for 2 h or 24 h. Representative blots are shown in (A). Quantifications of LRRK2 S935 phosphorylation are shown in (B) (2 h upper panel and 24 h lower panel). Graphs shows mean ± s.e.m. ($n \geq 3$ (except for PPP2R2B at 24 h $n = 2$)). Statistical significance was tested with column statistics with Bonferroni correction (*$P < 0.05$; ns = not significant). (C, D) SH-SY5Y cells stably expressing dCas9-KRAB were infected with lentivirus constructs expressing a negative control sgRNA or a sgRNA targeting phosphatase PPP2R2A. Cells were grown for at least 10 days and then analyzed for phosphatase levels, total LRRK2 levels, and phospho-Ser935 (D). β-Actin was used as the internal control. The data represent the outcomes of at least three biological replicate assays. Graphs show mean ± s.e.m. Statistical significance was tested with non-parametric Mann-Whitney *U* test one-tailed for phosphatase levels and two-tailed for LRRK2 levels and phospho-Ser935 levels ($^{\#,*}P < 0.05$; ns = not significant).

dephosphorylation at S935 albeit with a concomitant reduction in LRRK2 levels, while at 2 h treatment LRRK2 inhibitor induced dephosphorylation is not affected by the PPP2CA + PPP2R2A/B/C knockdown (Fig. 7A-B). To further confirm the implication of PP2A regulatory subunits on endogenous LRRK2 levels, we modulated the endogenous level of PPP2R2A via a genetic manipulation method, i.e. clustered interspaced short palindromic repeats (CRISPR) technology which can be used to direct transcriptional repressors or activators to specific genes for depletion or overexpression of the endogenous protein (Gilbert et al., 2013) in order to identify those that affect LRRK2 phosphorylation. We analyzed phosphorylation levels in SH-SY5Y cells stably expressing dCas9-KRAB (CRISPRi). Interestingly PPP2R2A CRISPRi induce an increase of endogenous LRRK2 phosphorylation (Fig. 7C, D). Taken together, these results suggest that phosphatase regulatory subunit PPP2R2A plays key role in LRRK2 phosphoregulation.

3.9. LRRK2 dephosphorylation induces LRRK2 protein destabilization and ubiquitination

Given our previous findings that LRRK2 kinase inhibitors can induce LRRK2 protein destabilization (Fig. 7B and reference (Lobbestael et al., 2016)), we set out to examine the effect of PPP2CA knock down on this phenomenon. Although reduced levels of the catalytic subunit PPP2CA alone did not affect inhibitor-induced LRRK2 protein destabilization 48 h after treatment, it resulted in a significant increase in LRRK2 protein levels in basal conditions (Fig. 8A, B).

We previously published that LRRK2 kinase inhibitor treatment induces dephosphorylation and ubiquitination of the protein (Zhao et al., 2015). As we also observed an effect of PP2A knockdown on LRRK2 protein levels (Fig. 8A, B) we wondered if the dephosphorylation observed in HEK-293 cells by reconstituted phosphatase holoenzymes (Fig. 2B) could induce LRRK2 ubiquitination. In cells expressing these effective PP2A holoenzymes (containing the regulatory subunits PPP2R2A/B/C/D), ubiquitination of LRRK2 was increased, while in cells expressing other PP2A holoenzyme combinations ubiquitination levels of LRRK2 were not significantly altered (Fig. 8C).

3.10. Expression levels of PP2A subunits in PD brains and in patient derived lymphoblastoid lines

In order to investigate clinical correlates for LRRK2 phosphatases, we verified whether their expression was altered in the brains of PD patients. Brain samples from a prior collaboration between Dr. Nichols and Dr. Dzamko/Dr. Halliday at the University of Sydney (Australia) (Dzamko et al., 2017) were tested for changes in expression levels of PP2A subunits (Fig. 9). These experiments revealed that the levels of

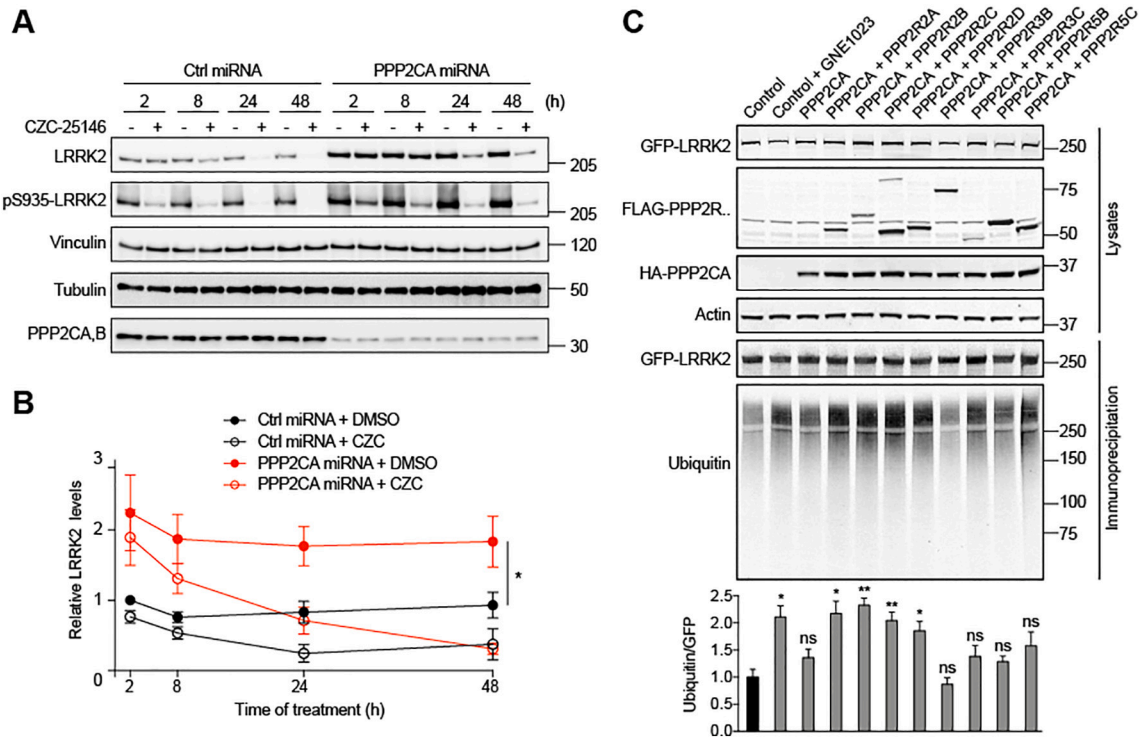

Fig. 8. PP2A affects LRRK2 protein level. (A, B) SH-SY5Y cells with stable expression of LRRK2 and stable knock down of PPP2CA were treated with LRRK2 kinase inhibitor for different periods of time as indicated. Representative blots are shown in panel (A). The graph in (B) shows the quantification of blots representing the ratio of total LRRK2 over housekeeping protein signal, relative to the control condition (solid black circles, Ctrl miRNA + DMSO at 2 h). Graph shows mean ± s.e.m. ($n = 3$). Statistical differences were tested by 2-way ANOVA using time and condition as factors, followed by Bonferroni *post-hoc* test to compare the effects of test groups against control group condition for each time point (*$P < 0.05$). (C) HEK-293 cells were transiently transfected with cDNAs encoding GFP-tagged LRRK2, HA-tagged catalytic PP2A subunits, and various FLAG-tagged regulatory PP2A subunits, as indicated. LRRK2 was immunoprecipitated with GFP-Trap_A beads, and ubiquitination was measured by immunoblotting. Graph shows mean ± s.e.m. (n = 3). Statistical significance tested with two-tailed *t*-test (*$P < 0.05$; **$P < 0.01$; ns = not significant).

PP2A regulatory (Fig. 9A) and catalytic (Fig. 9B) subunits were unchanged in three brain areas of PD patients compared to healthy controls (occipital cortex, frontal cortex, amygdala), with only the regulatory subunits showing a slight decrease in the substantia nigra. This is in agreement with an immunohistochemical study reporting no changes in PPP2CA/B and PPP2R2A/B/C/D levels in both cortical and substantia nigral samples of PD patients (Park et al., 2016). Similarly, a pilot study was performed in lysates of lymphoblastoid cell lines isolated from sporadic PD patients and controls as described previously (Fernández et al., 2019). LRRK2 S935 phosphorylation rates and PPP2CA levels were measured by western blot and our preliminary observations are a reduced LRRK2 phosphorylation as well as increased PPP2CA expression in sporadic patients compared to healthy controls (supplemental fig. 7).

4. Discussion

The phosphorylation state of LRRK2 at the ANK-LRR interdomain region containing the S910/S935/S955/S973 phosphorylation sites plays a central role in the normal function of LRRK2, governing LRRK2's subcellular localization. Furthermore, LRRK2 is dephosphorylated in PD patient brains (Dzamko et al., 2017) as are LRRK2 disease mutants expressed in mammalian cells and animal models (Nichols et al., 2010; Doggett et al., 2012; Lobbestael et al., 2013; Li et al., 2011), implicating LRRK2 dephosphorylation in the development of PD. In addition, LRRK2 kinase inhibition, a proposed PD therapeutic strategy, induces LRRK2 dephosphorylation. By consequence, identifying the phosphatases involved in LRRK2 dephosphorylation is important in understanding LRRK2 function in health and disease. Crucially, several phosphatases function as complexes called holoenzymes composed of a catalytic subunit and one or more additional subunits filling a regulatory or scaffolding role thus providing substrate specificity to the otherwise promiscuous catalytic subunit. In these cases, the identification of the LRRK2 phosphatase involves confirming the activity of a multiprotein complex. Here we present evidence showing that the phosphatase holoenzyme PPP2CA:PPP2R2 is a direct upstream regulator of LRRK2 phosphorylation at the ANK-LRR interdomain region.

Several pieces of evidence support the identification of PPP2CA:PPP2R2 as a LRRK2 phosphatase holoenzyme: (Zimprich et al., 2004) an unbiased siRNA primary screen; (Nichols et al., 2010) a secondary shRNA (Osório et al., 2014) and overexpression screen of 39 candidate phosphatases selected from the primary screen; (Simón-Sánchez et al., 2009) the recruitment of candidate phosphatases to the LRRK2 compartment in cells under dephosphorylation conditions; (Satake et al., 2009) reconstitution of the effects in vitro and in micro-injected oocytes with purified proteins; (Lill et al., 2012) the lack of inhibitor-induced LRRK2 dephosphorylation in conditions of combined knock down; (Healy et al., 2008) validation of a dephosphorylation dependent effect of LRRK2 ubiquitination via PPP2CA:PPP2R2; (Haugarvoll et al., 2008) validation of the effect of endogenous PPP2R2A on endogenous LRRK2 phosphorylation via expression modulation with CRISPR/dCas9.

Importantly, our study demonstrates that the dephosphorylation of LRRK2 by the PP2A complex depends on the presence of the regulatory subunits PPP2R2. In overexpression testing, we found that LRRK2 dephosphorylation in the presence of PP2A catalytic subunits alone was weak, however it is significantly increased for PP2A when PPP2R2A/B/C/D are co-expressed. These data are complemented by experiments with direct injection of purified phosphatases in *Xenopus* oocytes, a system with the benefit of overcoming the large time frame of plasmid or viral vector based overexpression experiments that require time for

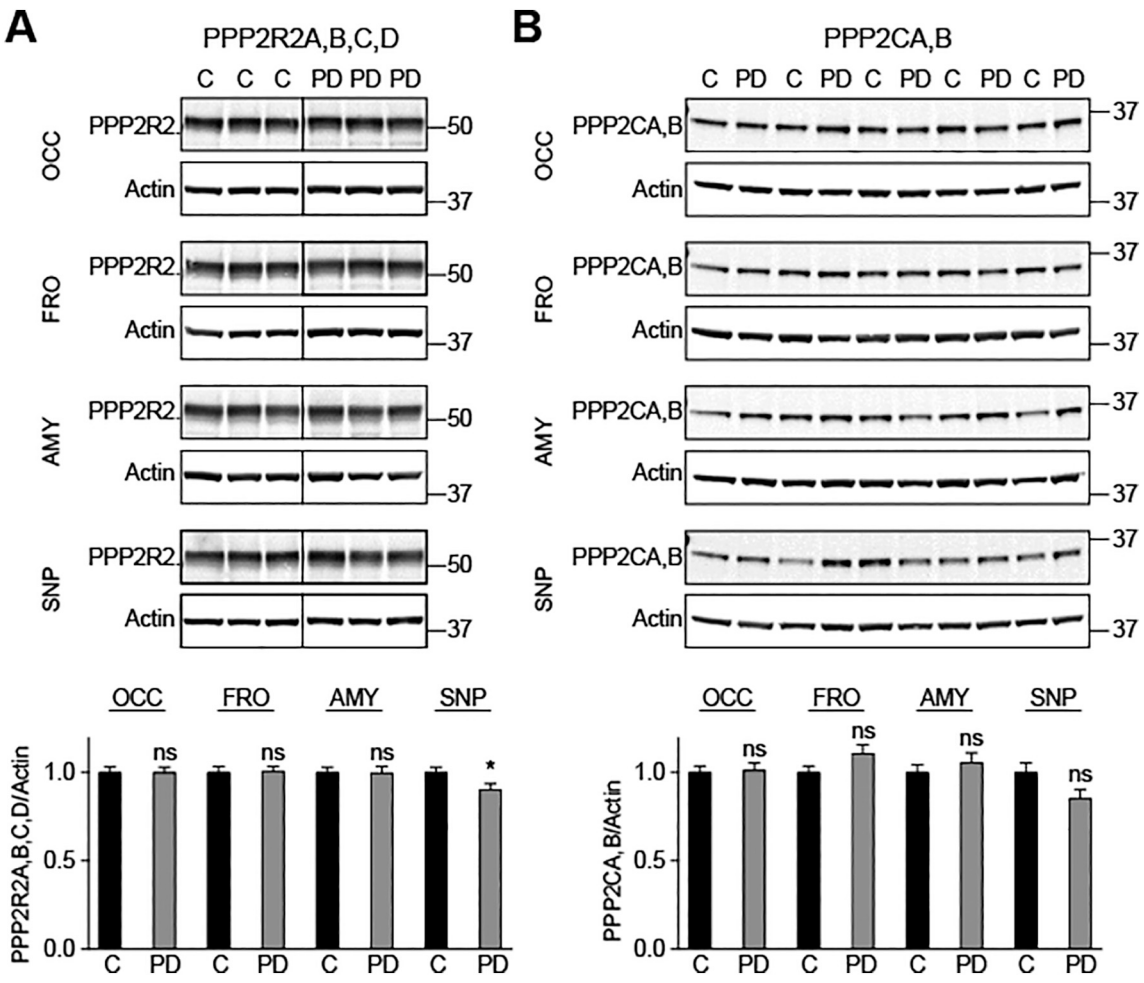

Fig. 9. Quantification of PP2A subunit expression levels in normal and PD brain. (A, B) Samples from four brain areas (OCC occipital cortex, FRO frontal cortex, AMY amygdala, SNP substantia nigra/putamen) from 25 PD patients and 25 healthy controls (C) were analyzed by immunoblotting. (A) Regulatory (PPP2R2A/B/C/D), and (B) catalytic (PPP2CA/B) subunits were visualized with specific antibodies. The figure shows representative blots. PP2A subunit levels were normalized to β-actin. Quantification revealed that the levels of all PP2A subunits were unchanged in brains from PD patients, except a slight decrease in PPP2R2 levels in the substantia nigra. Graphs show mean ± s.e.m. Statistical significance was tested with two-tailed t-test (*$P < 0.05$; ns = not significant).

transcription and translation steps. Using this technique, we observed that injection of the PPP2CA subunit alone was insufficient to dephosphorylate LRRK2, while the complementation of PPP2CA with regulatory subunits PPP2R2A/B produced robust LRRK2 dephosphorylation. Moreover, overexpression of the PP2A holoenzyme, but not PPP2CA subunit alone induced LRRK2 subcellular relocalization. These are indications that the combination of PPP2CA with PPP2R2A/B/C/D is a candidate phosphatase holoenzyme for LRRK2. These observations are also consistent with previous studies that have demonstrated that the PP2A holoenzyme is more effective to dephosphorylate specific target proteins (for example Tau protein) than the core dimer and even more than the PPP2CA alone (Goedert et al., 1992; Ferrigno et al., 1993; Xu et al., 2006).

It should be noted that previous work has reported a link between PP2A and LRRK2, without demonstrating a role for PP2A in LRRK2 dephosphorylation at the S935 cluster. For instance, PP2A has been identified as a genetic modulator of LRRK2 induced toxicity in a LRKR2 G2019S Drosophila model (Sim et al., 2020). Using an unbiased RNAi phosphatase screen in flies, the authors identified subunits *dPP2A-29B*, *mts* and *wrd*, corresponding to the scaffolding, catalytic and regulatory (PPP2R3) subunits of PP2A in humans, respectively. This study also demonstrated that PP2A overexpression led to a reduction of pS1292-level consistent with a previous study (Reynolds et al., 2014), however the effect on the S935 site was not reported so it is not possible to extend a correlation to our present study. These data nevertheless shed light on the role of the regulatory subunits that is directing the catalytic subunit to the specific substrate. Based on these studies and our present work, we can postulate that PPP2R2 will direct PPP2CA towards the pS935 phosphosite (Sim et al., 2020) while PPP2R3 would direct PPP2CA to the S1292 phosphosite of LRRK2.

The importance of the PP2A regulatory subunits PPP2R2 obtained in overexpression systems were confirmed for endogenous proteins in cells with neuronal phenotype. Here we show that reducing the endogenous levels of PPP2CA and PPP2R2A/B/C in SH-SY5Y neuroblastoma cells can prevent the LRRK2 dephosphorylation at S935, induced by 24 h of LRRK2 kinase inhibition, but not at 2 h of treatment. This is an interesting observation as we have previously shown that molecular inhibition of PP1 can prevent LRRK2 kinase inhibitor-induced dephosphorylation of LRRK2, after 30 min of treatment (Lobbestael et al., 2013). This might indicate that the very fast LRRK2 S935 dephosphorylation induced by inhibitor treatment is mediated by PP1, while PP2A holoenzymes are involved in the more sustained dephosphorylation during chronic inhibition, which is likely to be related to LRRK2 ubiquitination and degradation.

In addition, we used a CRISPR/dCas9-KRAB system to repress expression of endogenous phosphatase PPP2R2A in SH-SY5Y neuroblastoma cells coupled to analysis of endogenous LRRK2 phosphorylation. Interestingly, the decreased endogenous expression of PPP2R2A

led to an increase of pS935-LRRK2 level, confirming PPP2R2A as strong regulator of LRRK2 phosphorylation. This result also suggests a tight relationship between PPP2R2A expression and endogenous LRRK2 phosphorylation that merits further attention in future studies.

An important step in characterizing candidate LRRK2 phosphatases is to assess their ability to dephosphorylate LRRK2 directly in a cell-free system. Indeed, we previously tested LRRK2 dephosphorylation in vitro using commercial recombinant PP2A catalytic subunits and found only moderate dephosphorylation of LRRK2 at S910/S935/S955/S973 (Lobbestael et al., 2013). Here, we were able to repeat the in vitro dephosphorylation experiments using purified holoenzyme complexes that included the catalytic (PPP2CA/B) as well as the regulatory (PPP2R2D) and scaffolding subunits (PPP2R1A/B) of the PP2A complex and found robust dephosphorylation of LRRK2. This dephosphorylation is sensitive to the PP2A inhibitor okadaic acid, indicating that the PPP2CA:PPP2R2D holoenzyme is capable of directly dephosphorylating LRRK2. By contrast, recombinant CDC25C does not induce LRRK2 dephosphorylation in vitro, consistent with an indirect effect on LRRK2 dephosphorylation or the absence of an additional factor required for dephosphorylation of LRRK2 by CDC25 (Fig. 6C). Future research will be required to elucidate the signaling pathways that could induce CDC25 activity on LRRK2.

It is interesting to note that knockdown of the PP1 catalytic subunit PPP1CA did not yield significant changes in LRRK2 dephosphorylation under screen conditions (Table S1), despite our report that PPP1CA controls the LRRK2 phosphorylation cycle (Lobbestael et al., 2013). Indeed, we had shown that LRRK2 is dephosphorylated in vitro by PP1 and that pharmacological inhibition of PP1 modulates LRRK2 phosphorylation. Also, we previously found that PPP1CA was recruited to LRRK2 when dephosphorylation is pharmacologically induced using a LRRK2 kinase inhibitor as well as in the presence of constitutively dephosphorylated LRRK2 variants (N1437H, R1441G and Y1699C) (Lobbestael et al., 2013). Although several regulatory subunits of PP1 were identified in the present study, further testing did not provide sufficient evidence to confirm a functional interaction with the catalytic subunit to propose a LRRK2 active PP1 holoenzyme. Still, our study confirms the involvement of PP1 in LRRK2 dephosphorylation, as we observe the rapid recruitment of PPP1CA in conditions of LRRK2 dephosphorylation using colocalization and PLA analysis. Therefore, more research is needed to further define PP1 holoenzymes active on LRRK2.

The action of the PPP2CA:PPP2R2 complex on LRRK2 dephosphorylation is also supported by the recruitment of the phosphatase subunits to the LRRK2 complex in intact cells under dephosphorylation conditions. Assessing colocalization under dephosphorylation conditions via immunocytochemistry (at 1 h after pharmacological dephosphorylation induction) or using videomicroscopy, has shown an increase in relocalization to the LRRK2 compartment for both PP1 and PP2A subunits. The videomicroscopy revealed that this relocalization was detectable within minutes after application of LRRK2 kinase inhibitor for PPP1CA and after approximately 30 min for PPP2CA, further suggesting that PP2A may have slightly slower kinetics for LRRK2 dephosphorylation compared to PP1. The rapid changing of colocalization is accompanied with an enhanced interaction between LRRK2 and PPP1CA, PPP2CA, PPP2R2A and PP2R2B after acute inhibition with two different LRRK2 kinase inhibitors. We and others have previously identified PPP1CA (Lobbestael et al., 2013) as well as PPP2R1A and PPP2CA (Athanasopoulos et al., 2016; Sim et al., 2020) as interacting proteins of LRRK2, and those findings are confirmed in the present study. Considering that physical interaction with their cognate phosphatases may be a hallmark of all dephosphorylation substrates (Virshup and Shenolikar, 2009), these data support the conclusion that LRRK2 is a true substrate for both PPP1CA and PPP2CA.

Recent reports have suggested that LRRK2 ubiquitination is related to LRRK2 dephosphorylation (Zhao et al., 2015) and that sustained LRRK2 kinase inhibition alters steady state LRRK2 expression levels (Lobbestael et al., 2016; Zhao et al., 2015; Fuji et al., 2015). Therefore, we tested whether the phosphatases dephosphorylating LRRK2 would induce the ubiquitination of LRRK2, and found that this was indeed the case (Fig. 8C). Conversely, our results show that the double knockdown of PP2A catalytic and regulatory subunits (Fig. 7A, B) or knock-down of PPP2CA alone (Fig. 8A, B) affect the level of LRRK2 by increasing LRRK2 levels. Our results therefore show an interplay between LRRK2 phosphorylation and LRRK2 ubiquitination/stability, suggesting that LRRK2 can be placed in the class of molecules and pathways regulated by the interplay of phosphorylation and ubiquitination (Hunter, 2007) in which phosphatases regulate both phosphorylation and expression levels of LRRK2.

Dzamko and colleagues previously reported a decrease in LRRK2 phosphorylation in PD brain (Dzamko et al., 2017). Therefore, one hypothesis is that this may be due to altered expression of LRRK2 phosphatase holoenzymes in PD brain. We tested PP2A expression levels in these post-mortem PD brain samples and found no changes in PPP2CA/B and PPP2R2A/B/C/D protein levels in PD versus control brains with the exception of the substantia nigra where a slight decrease in PP2A regulatory subunit levels was observed. A precedent study by Park and colleagues also observed no changes in total PPP2CA/B and total PPP2R2A/B/C/D subunits in PD and dementia with Lewy body (DLB) brains (Park et al., 2016); the authors also demonstrated a markedly decreased expression of methylated PP2A leading to reduced PP2A activity. In addition to brain, LRRK2 is also known to be highly expressed in other tissues (lung, kidney, spleen, peripheral blood cells), while PP2A subunits are not uniformly expressed all across the human body. In fact, PP2A regulatory subunits PPP2R2A and PPP2R2D have a wide-spread tissue distribution similar to LRRK2 (Janssens and Goris, 2001), while the expression of PPP2R2B (testis, brain) and PPP2R2C (only brain) is much more restricted (Strack et al., 1998; Dagda et al., 2003). Our own preliminary results in a pilot study in human patient lymphoblastoid cells suggest a dephosphorylation of LRRK2 together with an upregulation of PPP2CA in these cells. Therefore, further research on LRRK2 phosphatases in PD should investigate PP2A holoenzyme activity in disease brains as well as expression and activity of phosphatases in extracerebral tissues.

It is interesting to speculate whether the findings from our study may be linked to other partners in the LRRK2 pathway. For instance several RAB proteins including RAB8A, RAB10, RAB29 are reported as bona fide substrates of LRRK2 (Ito et al., 2016; Steger et al., 2016; Steger et al., 2017; Liu et al., 2017; Thirstrup et al., 2017; Purlyte et al., 2018). In that regard, Sacco et al have shown that the PPP2CA-PPP2R1A dimer can be disrupted by RAB8 and RAB9 proteins and represent a novel molecular mechanism to regulate the catalytic activity of the PP2A holoenzyme in different subcellular compartments (Sacco et al., 2016). This opens the possibility of a potential mutually regulatory mechanism whereby LRRK2 could regulate its own phosphorylation level via the regulation of PP2A by its RAB substrates.

5. Conclusions

In summary, our unbiased search for LRRK2 phosphatases confirms the involvement of PP1 in LRRK2 dephosphorylation and reveals the PP2A complex PPP2CA:PPP2R2 as a key physiological upstream regulator of LRRK2. Crucially, the catalytic subunit PPP2CA is rather inefficient at dephosphorylating LRRK2, while complementation with the PPP2R2 regulatory subunit elicits a robust LRRK2 dephosphorylation and change in LRRK2 subcellular localization. In the summary of the proposed mechanism, both PPP1CA and the PPP2CA:PPP2R2 complex are recruited to LRRK2 under dephosphorylation conditions. In addition to dephosphorylating LRRK2, this PP2A holoenzyme induces LRRK2 ubiquitination and affect LRRK2 expression levels, suggesting that the PPP2CA:PPP2R2 complex plays a key role in LRRK2 function by priming LRRK2 for degradation via its dephosphorylation. The identification of the PPP2CA:PPP2R2 complex regulating LRRK2 S910/S935/S955/S973

phosphorylation paves the way for studies refining PD therapeutic strategies that impact LRRK2 phosphorylation, including patient stratification based on phosphatase expression, understanding interindividual variability in LRRK2 dephosphorylation after LRRK2 kinase inhibitor treatment or developing novel strategies based on targeting the LRRK2 phosphoregulation complex.

Supplementary data to this article can be found online at https://doi.org/10.1016/j.nbd.2021.105426.

Authors' contributions

RJN and J-MT conceived the project; M-CC-H, VB, RJN. and J-MT designed and supervised the project; MFB, MD, EL, ME, M-CC-H, VB, RJN and J-MT wrote the paper; MFB performed and analyzed the secondary screen via overexpression of phosphatases, in vitro dephosphorylation experiments, LRRK2 ubiquitination experiments and analysis of post-mortem human brain samples; MD performed and analyzed immunofluorescence, PLA and CRISPR experiments; EL performed and analyzed the secondary knockdown screen; EL and TDW performed and analyzed the LRRK2 stability experiments; RL, ME, MD, AM, KC and J-FB contributed to the Xenopus oocyte experiment; CVDH. and J-MT designed the lentiviral vectors used in the study; ME performed and analyzed videomicroscopy experiments; WS produced LRRK2 recombinant protein standards. CL, MD, MCCH and EM contributed to the collection and analysis of patient derived lymphoblastoid cells. All authors read and approved the manuscript.

Funding

The work was funded by the Michael J. Fox Foundation (grants 06709, 06709.01, 06709.02, 06709.03). Support from the KU Leuven, Flanders Innovation & Entrepreneurship (VLAIO) (doctoral fellowship TDW IWT.141396), Research Foundation Flanders (FWO, projects G0E1917N and SBOS006617N), the researcher attraction program of the Nord Pas-de-Calais Region (currently Hauts de France Region, France, Individual fellowship to J-MT), the Doctoral School Biology Health of Lille (doctoral scholarship to MD), French Ministry of Health's PHRC program (CONVERGENCE 2008-A00219–42), Inserm, Université de Lille, CHU de Lille is gratefully acknowledged. RJN is funded by the gracious support of The Alexander and Eva Nemeth Foundation. This project has received funding from the European Union's Horizon 2020 research and innovation programme under grant agreement No 659183 (Marie Sklodowska-Curie individual fellowship to J-MT, project RECOLOR).

Ethics approval

Experiments using human brain tissue lysates were approved by the University of NSW Human Research Ethics Advisory (#HC14046).

Declaration of Competing Interest

The authors declare that they have no competing interests.

Acknowledgements

The authors gratefully acknowledge the support of several technological platforms and core facilities, including the Bio Imaging Center Lille (BiCEL, www.bicel.org), the Leuven viral vector core (www.lvvc.be) and the Lille Neuroscience & Cognition viral vector facility. Portions of this project were initiated at The Parkinson's Institute and were finished at Stanford University School of Medicine. We acknowledge the Sydney Brain Bank at Neuroscience Research Australia and the Brain Bank for Aging Research at the Tokyo Metropolitan Geriatric hospital for supply of brain tissue to access to post-mortem brain samples. The authors thank Christel Vanbesien, Karim Belarbi, Malika Hamdane and Robert-Alain Toillon for fruitful discussions and also acknowledge the technical and logistical support of Thomas Comptdaer, Pierre Semaille, Fangye Gao and Stephanie Deman.

References

Adams, D.G., Wadzinski, B.E., 2007. Isolation and characterization of PP2A holoenzymes containing FLAG-tagged B subunits. Methods Mol. Biol. 365, 101–111.
Athanasopoulos, P.S., Jacob, W., Neumann, S., Kutsch, M., Wolters, D., Tan, E.K., et al., 2016 Jun 1. Identification of protein phosphatase 2A as an interacting protein of leucine-rich repeat kinase 2. Biol. Chem. 397 (6), 541–554.
de Broucker, A., Semaille, P., Cailliau, K., Martoriati, A., Comptdaer, T., Bodart, J.-F., et al., 2015. Xenopus laevis as a model to identify translation impairment. J. Vis. Exp. 103, 1–9.
Chia, R., Haddock, S., Beilina, A., Rudenko, I.N., Mamais, A., Kaganovich, A., et al., 2014 Jan 15. Phosphorylation of LRRK2 by casein kinase 1α regulates trans-Golgi clustering via differential interaction with ARHGEF7. Nat. Commun. 5, 5827 (Nature Publishing Group).
Choi, H.G., Zhang, J., Deng, X., Hatcher, J.M., Patricelli, M.P., Zhao, Z., et al., 2012 Aug 9. Brain penetrant LRRK2 inhibitor. ACS Med. Chem. Lett. 3 (8), 658–662.
Civiero, L., Vancraenenbroeck, R., Belluzzi, E., Beilina, A., Lobbestael, E., Reyniers, L., et al., 2012 Jan. Biochemical characterization of highly purified leucine-rich repeat kinases 1 and 2 demonstrates formation of homodimers. PLoS One 7 (8), e43472.
Dagda, R.K., Zaucha, J.A., Wadzinski, B.E., Strack, S., 2003 Jul. A developmentally regulated, neuron-specific splice variant of the variable subunit Bbeta targets protein phosphatase 2A to mitochondria and modulates apoptosis. J. Biol. Chem. 278 (27), 24976–24985.
Daniëls, V., Vancraenenbroeck, R., Law, B.M.H., Greggio, E., Lobbestael, E., Gao, F., et al., 2011 Jan. Insight into the mode of action of the LRRK2 Y1699C pathogenic mutant. J. Neurochem. 116 (2), 304–315.
Deng, X., Dzamko, N., Prescott, A., Davies, P., Liu, Q., Yang, Q., et al., 2011 Apr. Characterization of a selective inhibitor of the Parkinson's disease kinase LRRK2. Nat. Chem. Biol. 7 (4), 203–205 (Nature Publishing Group).
Di Maio, R., Hoffman, E.K., Rocha, E.M., Keeney, M.T., Sanders, L.H., De Miranda, B.R., et al., 2018. LRRK2 activation in idiopathic Parkinson's disease. Sci. Transl. Med. 10 (451).
Doggett, E.A., Zhao, J., Mork, C.N., Hu, D., Nichols, R.J., 2012 Jan. Phosphorylation of LRRK2 serines 955 and 973 is disrupted by Parkinson's disease mutations and LRRK2 pharmacological inhibition. J. Neurochem. 120 (1), 37–45.
Dzamko, N., Deak, M., Hentati, F., Reith, A.D., Prescott, A.R., Alessi, D.R., et al., 2010 Sep 15. Inhibition of LRRK2 kinase activity leads to dephosphorylation of Ser(910)/Ser(935), disruption of 14-3-3 binding and altered cytoplasmic localization. Biochem. J. 430 (3), 405–413.
Dzamko, N., Inesta-Vaquera, F., Zhang, J., Xie, C., Cai, H., Arthur, S., et al., 2012 Jan. The IkappaB kinase family phosphorylates the Parkinson's disease kinase LRRK2 at Ser935 and Ser910 during toll-like receptor signaling. PLoS One 7 (6), e39132.
Dzamko, N., Gysbers, A.M., Bandopadhyay, R., Bolliger, M.F., Uchino, A., Zhao, Y., et al., 2017 Mar. LRRK2 levels and phosphorylation in Parkinson's disease brain and cases with restricted Lewy bodies. Mov. Disord. 32 (3), 423–432.
Fell, M.J., Mirescu, C., Basu, K., Cheewatrakoolpong, B., DeMong, D.E., Ellis, J.M., et al., 2015 Dec. MLi-2, a potent, selective, and centrally active compound for exploring the therapeutic potential and safety of LRRK2 kinase inhibition. J. Pharmacol. Exp. Ther. 355 (3), 397–409.
Fernández, B., Lara Ordóñez, A.J., Fdez, E., Mutez, E., Comptdaer, T., Leghay, C., et al., 2019. Centrosomal cohesion deficits as cellular biomarker in lymphoblastoid cell lines from LRRK2 Parkinson's disease patients. Biochem. J. 476 (19).
Ferrigno, P., Langan, T.A., Cohen, P., 1993 Jul. Protein phosphatase 2A1 is the major enzyme in vertebrate cell extracts that dephosphorylates several physiological substrates for cyclin-dependent protein kinases. Mol. Biol. Cell 4 (7), 669–677.
Forrest, A.R.R., Kawaji, H., Rehli, M., Baillie, J.K., De Hoon, M.J.L., Haberle, V., et al., 2014 Mar. A promoter-level mammalian expression atlas. Nature 507 (7493), 462–470 (Nature Publishing Group).
Fuji, R.N., Flagella, M., Baca, M.A., Baptista, M.A., Brodbeck, J., Chan, B.K., et al., 2015 Feb 4. Effect of selective LRRK2 kinase inhibition on nonhuman primate lung. Sci. Transl. Med. 7 (273), 273ra15.
Gilbert, L.A., Larson, M.H., Morsut, L., Liu, Z., Brar, G.A., Torres, S.E., et al., 2013 Jul 18. CRISPR-mediated modular RNA-guided regulation of transcription in eukaryotes. Cell. 154 (2), 442–451 (Elsevier Inc.).
Gloeckner, C.J., Boldt, K., von Zweydorf, F., Helm, S., Wiesent, L., Sarioglu, H., et al., 2010 Apr 5. Phosphopeptide analysis reveals two discrete clusters of phosphorylation in the N-terminus and the roc domain of the Parkinson-disease associated protein kinase LRRK2. J. Proteome Res. 9 (4), 1738–1745.
Goedert, M., Cohen, E.S., Jakes, R., Cohen, P., 1992 Nov. p42 MAP kinase phosphorylation sites in microtubule-associated protein tau are dephosphorylated by protein phosphatase 2A1. Implications for Alzheimer's disease [corrected]. FEBS Lett. 312 (1), 95–99.
Häbig, K., Walter, M., Poths, S., Riess, O., Bonin, M., 2008 May. RNA interference of LRRK2-microarray expression analysis of a Parkinson's disease key player. Neurogenetics. 9 (2), 83–94.
Haugarvoll, K., Rademakers, R., Kachergus, J.M., Nuytemans, K., Ross, O.A., Gibson, J. M., et al., 2008. Lrrk2 R1441C parkinsonism is clinically similar to sporadic Parkinson disease. Neurology 70 (16 PART 2), 1456–1460 (Lippincott Williams and Wilkins).

Healy, D.G., Falchi, M., O'Sullivan, S.S., Bonifati, V., Durr, A., Bressman, S., et al., 2008 Jul. Phenotype, genotype, and worldwide genetic penetrance of LRRK2-associated Parkinson's disease: a case-control study. Lancet Neurol. 7 (7), 583–590.
Henderson, J.L., Kormos, B.L., Hayward, M.M., Coffman, K.J., Jasti, J., Kurumbail, R.G., et al., 2015 Jan 8. Discovery and preclinical profiling of 3-[4-(morpholin-4-yl)-7H-pyrrolo[2,3-d]pyrimidin-5-yl]benzonitrile (PF-06447475), a highly potent, selective, brain penetrant, and in vivo active LRRK2 kinase inhibitor. J. Med. Chem. 58 (1), 419–432.
Hermanson, S.B., Carlson, C.B., Riddle, S.M., Zhao, J., Vogel, K.W., Nichols, R.J., et al., 2012 Jan. Screening for novel LRRK2 inhibitors using a high-throughput TR-FRET cellular assay for LRRK2 Ser935 phosphorylation. PLoS One 7 (8), e43580.
Hsu, P.D., Lander, E.S., Zhang, F., 2014 Jun. Development and applications of CRISPR-Cas9 for genome engineering. Cell. 157 (6), 1262–1278 (Elsevier).
Hunter, T., 2007 Dec. The age of crosstalk: phosphorylation, ubiquitination, and beyond. Mol. Cell 28 (5), 730–738.
Ito, G., Okai, T., Fujino, G., Takeda, K., Ichijo, H., Katada, T., et al., 2007 Feb 6. GTP binding is essential to the protein kinase activity of LRRK2, a causative gene product for familial Parkinson's disease. Biochemistry. 46 (5), 1380–1388.
Ito, G., Fujimoto, T., Kamikawaji, S., Kuwahara, T., Iwatsubo, T., 2014 Jan. Lack of correlation between the kinase activity of LRRK2 harboring kinase-modifying mutations and its phosphorylation at Ser910, 935, and Ser955. PLoS One 9 (5), e97988.
Ito, G., Katsemonova, K., Tonelli, F., Lis, P., Baptista, M.A.S., Shpiro, N., et al., 2016 Sep 1. Phos-tag analysis of Rab10 phosphorylation by LRRK2: a powerful assay for assessing kinase function and inhibitors. Biochem. J. 473 (17), 2671–2685.
Janssens, V., Goris, J., 2001 Feb. Protein phosphatase 2A: a highly regulated family of serine/threonine phosphatases implicated in cell growth and signalling. Biochem. J. 353 (Pt 3), 417–439.
Janssens, V., Longin, S., Goris, J., 2008 Mar. PP2A holoenzyme assembly: in cauda venenum (the sting is in the tail). Trends Biochem. Sci. 33 (3), 113–121.
Kalogeropulou, A.F., Zhao, J., Bolliger, M.F., Memou, A., Narasimha, S., Molitor, T.P., et al., 2018 Apr 9. P62/SQSTM1 is a novel leucine-rich repeat kinase 2 (LRRK2) substrate that enhances neuronal toxicity. Biochem. J. 475 (7), 1271–1293.
Kiely, M., Kiely, P.A., 2015 Apr 10. PP2A: the wolf in sheep's clothing? Cancers (Basel). 7 (2), 648–669.
Li, X., Wang, Q.J., Pan, N., Lee, S., Zhao, Y., Chait, B.T., et al., 2011 Jan. Phosphorylation-dependent 14-3-3 binding to LRRK2 is impaired by common mutations of familial Parkinson's disease. PLoS One 6 (3), e17153.
Lill, C.M., Roehr, J.T., McQueen, M.B., Kavvoura, F.K., Bagade, S., Schjeide, B.-M.M., et al., 2012 Jan. Comprehensive research synopsis and systematic meta-analyses in Parkinson's disease genetics: the PDGene database. PLoS Genet. 8 (3), e1002548.
Liu, Z., Lee, J., Krummey, S., Lu, W., Cai, H., Lenardo, M.J., 2011 Nov. The kinase LRRK2 is a regulator of the transcription factor NFAT that modulates the severity of inflammatory bowel disease. Nat. Immunol. 12 (11), 1063–1070.
Liu, Z., Bryant, N., Kumaran, R., Beilina, A., Abeliovich, A., Cookson, M.R., et al., 2017. LRRK2 phosphorylates membrane-bound Rabs and is activated by GTP-bound Rab7L1 to promote recruitment to the trans-Golgi network. Hum. Mol. Genet. 27 (2), 385–395.
Lobbestael, E., Reumers, V., Ibrahimi, A., Paesen, K., Thiry, I., Gijsbers, R., et al., 2010 Jan. Immunohistochemical detection of transgene expression in the brain using small epitope tags. BMC Biotechnol. 10, 16.
Lobbestael, E., Zhao, J., Rudenko, I.N., Beylina, A., Gao, F., Wetter, J., et al., 2013 Nov 15. Identification of protein phosphatase 1 as a regulator of the LRRK2 phosphorylation cycle. Biochem. J. 456 (1), 119–128.
Lobbestael, E., Civiero, L., De Wit, T., Taymans, J.-M., Greggio, E., Baekelandt, V., 2016 Sep 23. Pharmacological LRRK2 kinase inhibition induces LRRK2 protein destabilization and proteasomal degradation. Sci. Rep. 6 (August 2015), 33897.
Marchand, A., Drouyer, M., Sarchione, A., Chartier-Harlin, M.C., Taymans, J.M., 2020. LRRK2 phosphorylation, more than an epiphenomenon. Front. Neurosci. 14 (13), 4646–4656.e4.
Mata, I.F., Wedemeyer, W.J., Farrer, M.J., Taylor, J.P., Gallo, K., 2006 May. a. LRRK2 in Parkinson's disease: protein domains and functional insights. Trends Neurosci. 29 (5), 286–293.
Nichols, R.J., Dzamko, N., Morrice, N.A., Campbell, D.G., Deak, M., Ordureau, A., et al., 2010 Sep 15. 14-3-3 binding to LRRK2 is disrupted by multiple Parkinson's disease-associated mutations and regulates cytoplasmic localization. Biochem. J. 430 (3), 393–404.
Osório, L., Gijsbers, R., Oliveras-Salvá, M., Michiels, A., Debyser, Z., Van den Haute, C., et al., 2014 Jan 16. Viral vectors expressing a single microRNA-based short-hairpin RNA result in potent gene silencing in vitro and in vivo. J. Biotechnol. 169 (1), 71–81 (Elsevier B.V.).
Park, H.-J., Lee, K.-W., Park, E.S., Oh, S., Yan, R., Zhang, J., et al., 2016. Dysregulation of protein phosphatase 2A in parkinson disease and dementia with lewy bodies. Ann. Clin. Transl. Neurol. 3 (10), 769–780.
Purlyte, E., Dhekne, H.S., Sarhan, A.R., Gomez, R., Lis, P., Wightman, M., et al., 2018 Jan. Rab29 activation of the Parkinson's disease-associated LRRK2 kinase. EMBO J. 37 (1), 1–18.
Radzisheuskaya, A., Shlyueva, D., Müller, I., Helin, K., 2016. Optimizing sgRNA position markedly improves the efficiency of CRISPR/dCas9-mediated transcriptional repression. Nucleic Acids Res. 44 (18), 4646–4656.e4.
Ramsden, N., Perrin, J., Ren, Z., Lee, B.D., Zinn, N., Dawson, V.L., et al., 2011 Oct 21. Chemoproteomics-based design of potent LRRK2-selective lead compounds that attenuate Parkinson's disease-related toxicity in human neurons. ACS Chem. Biol. 6 (10), 1021–1028.
Reyniers, L., Del Giudice, M.G., Civiero, L., Belluzzi, E., Lobbestael, E., Beilina, A., et al., 2014 Jun 20. Differential protein-protein interactions of LRRK1 and LRRK2 indicate roles in distinct cellular signaling pathways. J. Neurochem. 131 (2), 239–250.
Reynolds, A., Doggett, E.A., Riddle, S.M., Lebakken, C.S., Nichols, R.J., 2014 Jun 24. LRRK2 kinase activity and biology are not uniformly predicted by its autophosphorylation and cellular phosphorylation site status. Front. Mol. Neurosci. 7 (June), 54.
Sacco, F., Mattioni, A., Boldt, K., Panni, S., Santonico, E., Castagnoli, L., et al., 2016. A subset of RAB proteins modulates PP2A phosphatase activity. Sci. Rep. 6, 32857.
Satake, W., Nakabayashi, Y., Mizuta, I., Hirota, Y., Ito, C., Kubo, M., et al., 2009 Dec. Genome-wide association study identifies common variants at four loci as genetic risk factors for Parkinson's disease. Nat. Genet. 41 (12), 1303–1307.
Schmitz, M.H.A., Held, M., Janssens, V., Hutchins, J.R.A., Hudecz, O., Ivanova, E., et al., 2010 Sep. Live-cell imaging RNAi screen identifies PP2A-B55alpha and importin-beta1 as key mitotic exit regulators in human cells. Nat. Cell Biol. 12 (9), 886–893 (Nature Publishing Group).
Scott, J.D., DeMong, D.E., Greshock, T.J., Basu, K., Dai, X., Harris, J., et al., 2017 Apr 13. Discovery of a 3-(4-Pyrimidinyl) Indazole (MLi-2), an orally available and selective leucine-rich repeat kinase 2 (LRRK2) inhibitor that reduces brain kinase activity. J. Med. Chem. 60 (7), 2983–2992.
Sheng, Z., Zhang, S., Bustos, D., Kleinheinz, T., Le Pichon, C.E., Dominguez, S.L., et al., 2012 Dec 12. Ser1292 autophosphorylation is an indicator of LRRK2 kinase activity and contributes to the cellular effects of PD mutations. Sci. Transl. Med. 4 (164), 164ra161.
Sim, J.P.L., Ziyin, W., Basil, A.H., Lin, S., Chen, Z., Zhang, C., et al., 2020 Oct 29. Identification of PP2A and S6 kinase as modifiers of leucine-rich repeat kinase-induced neurotoxicity. NeuroMolecular Med. 22 (2), 218–226 (Springer US).
Simón-Sánchez, J., Schulte, C., Bras, J.M., Sharma, M., Gibbs, J.R., Berg, D., et al., 2009 Dec. Genome-wide association study reveals genetic risk underlying Parkinson's disease. Nat. Genet. 41 (12), 1308–1312 (Nature Publishing Group).
Steger, M., Tonelli, F., Ito, G., Davies, P., Trost, M., Vetter, M., et al., 2016 Jan 29. Phosphoproteomics reveals that Parkinson's disease kinase LRRK2 regulates a subset of Rab GTPases. Elife. 5 (January), 1–28.
Steger, M., Diez, F., Dhekne, H.S., Lis, P., Nirujogi, R.S., Karayel, O., et al., 2017. Systematic proteomic analysis of LRRK2-mediated rab GTPase phosphorylation establishes a connection to ciliogenesis. Elife 6 (13), 4646–4656.e4.
Strack, S., Zaucha, J.A., Ebner, F.F., Colbran, R.J., Wadzinski, B.E., 1998 Mar. Brain protein phosphatase 2A: developmental regulation and distinct cellular and subcellular localization by B subunits. J. Comp. Neurol. 392 (4), 515–527.
Taymans, J.-M., Greggio, E., 2016. LRRK2 kinase inhibition as a therapeutic strategy for Parkinson's disease, where do we stand? Curr. Neuropharmacol. 14 (3), 214–225.
Taymans, J.-M., Gao, F., Baekelandt, V., 2013 Jan. Metabolic labeling of leucine rich repeat kinases 1 and 2 with radioactive phosphate. J. Vis. Exp. 79, e50523.
Thirstrup, K., Dächsel, J.C., Oppermann, F.S., Williamson, D.S., Smith, G.P., Fog, K., et al., 2017 Aug 31. Selective LRRK2 kinase inhibition reduces phosphorylation of endogenous Rab10 and Rab12 in human peripheral mononuclear blood cells. Sci. Rep. 7 (1), 10300.
Vancraenenbroeck, R., De Raeymaecker, J., Lobbestael, E., Gao, F., De Maeyer, M., Voet, A., et al., 2014 Jan 3. In silico, in vitro and cellular analysis with a kinome-wide inhibitor panel correlates cellular LRRK2 dephosphorylation to inhibitor activity on LRRK2. Front. Mol. Neurosci. 7 (June), 51.
Virshup, D.M., Shenolikar, S., 2009. From promiscuity to precision: protein phosphatases get a makeover. Mol. Cell 33 (5), 537–545 (Elsevier Inc.).
Xu, Y., Xing, Y., Chen, Y., Chao, Y., Lin, Z., Fan, E., et al., 2006. Structure of the protein phosphatase 2A holoenzyme. Cell. 127 (6), 1239–1251.
Zhao, J., Molitor, T.P., Langston, J.W., Nichols, R.J., 2015 May 5. LRRK2 Dephosphorylation increases its ubiquitination. Biochem. J. May, 107–120.
Zimprich, A., Biskup, S., Leitner, P., Lichtner, P., Farrer, M., Lincoln, S., et al., 2004 Nov 18. Mutations in LRRK2 cause autosomal-dominant parkinsonism with pleomorphic pathology. Neuron. 44 (4), 601–607.